AD-A113 249 FLORIDA UNIV GAINESVILLE DEPT OF ENGINEERING SCIENCES F/G 11/4
STUDIES ON THE FRACTURE MECHANISMS IN PARTIALLY PENETRATED FILA--ETC(U)
JAN 82 R L SIERAKOWSKI, C A ROSS, L E MALVERN DAAG29-79-G-0007
UNCLASSIFIED TR-1 ARO-15989.8-E NL

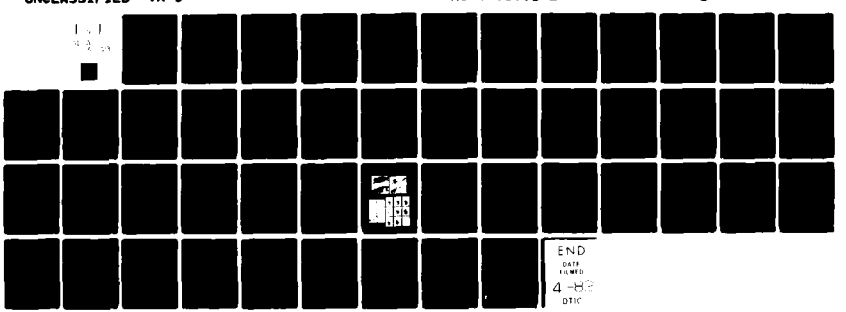

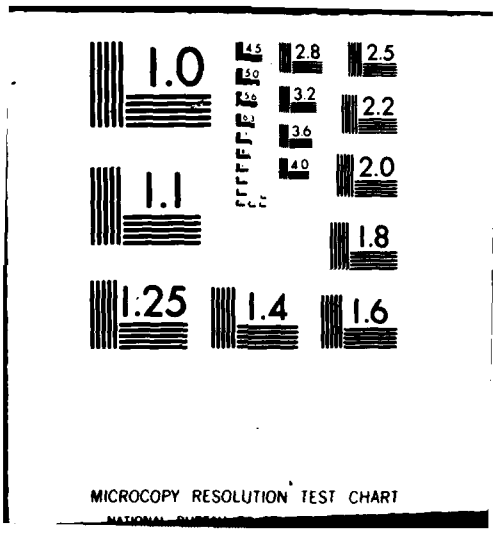
1.0
1.1
1.25
1.4
1.6
1.8
2.0
2.2
2.5
2.8
3.2
3.6
4.0
4.5
5.0
5.6
MICROCOPY RESOLUTION TEST CHART

ARO 15989.8-E

(12)

STUDIES ON THE FRACTURE MECHANISMS IN PARTIALLY PENETRATED FILAMENT REINFORCED LAMINATED PLATES

TECHNICAL REPORT NO. 1

R.L. SIERAKOWSKI
C.A. ROSS
L.E. MALVERN
H.W. DODDINGTON

JANUARY 30, 1982

U.S. ARMY RESEARCH OFFICE

DAAG29-79-G-0007

UNIVERSITY OF FLORIDA

APPROVED FOR PUBLIC RELEASE;
DISTRIBUTION UNLIMITED.

STUDIES ON THE FRACTURE MECHANISMS IN PARTIALLY PENETRATED FILAMENT REINFORCED LAMINATED PLATES

Technical Report No. 1

R.L. Sierakowski

C.A. Ross

L.E. Malvern

H.W. Doddington

January 30, 1982

U.S. Army Research Office

Grant No.

DAAG29-79-G-0007

University of Florida

Approved for Public Release:

Distribution Unlimited

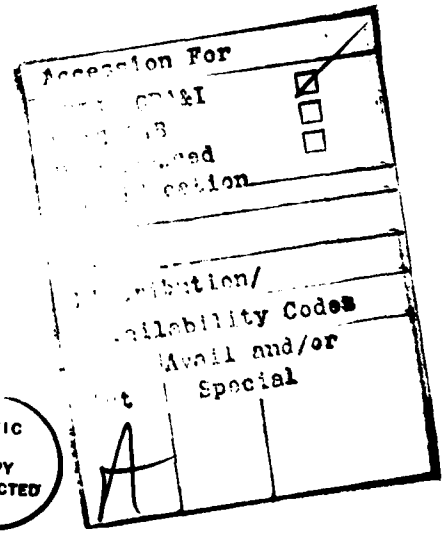

THE VIEWS, OPINIONS, AND/OR FINDINGS CONTAINED IN THIS REPORT ARE THOSE OF THE AUTHORS AND SHOULD NOT BE CONSTRUED AS AN OFFICIAL DEPARTMENT OF THE ARMY POSITION, POLICY, OR DECISION, UNLESS SO DESIGNATED BY OTHER DOCUMENTATON

ABSTRACT

The overall objective of this research program has been to obtain information on the fracture mechanisms occurring in centrally impacted composite plates in order to establish design guidelines for plates to resist such impacts. Topics investigated but not previously reported in journal articles are included in this report, as summarized the following three paragraphs.

An 8-channel transient recorder system was designed, built and tested. The system uses charge-coupled analog shift registers (CCD registers) to sample and temporarily store transient signals (lasting 0.1 to 1 millisec) in analog form. The signals are then read out at a slower rate, digitized and stored in a microprocessor system with a dual floppy disk memory, a video terminal and a printer. It is expected that the system will serve in this laboratory for many years for recording transient wave propagation events resulting from impact on composite plates or other structural elements. Market changes during the development of this system may make direct analog-to-digital conversion of the transient signals an economically competitive system for sampling rates of 1 to 10 MHz, although the system using CCD registers still seems attractive for sampling rates of 10 to 100 MHz.

A three dimensional orthotropic-material elastic analysis was performed to calculate the interlaminar shear stress in a $[0°_5/90°_5/0°_5]$ glass/epoxy plate under central loading simulating a center point normal impact at 45.7 m/s (150 ft/sec) by a steel cylinder of diameter 9.7 mm and length 25.4 mm. The calculation was performed with the SAP IV finite-element computer code. Results indicated a considerable region where the estimated interlaminar shear strength was exceeded. Thus delamination would be expected to occur, as experimental studies have confirmed. The experimental delaminated areas do not correlate directly with the areas where the shear strength was exceeded in the elastic solution, because the stress distribution is altered during the delamination, which was not accounted for in the elastic solution.

Static three-point cylindrical bending tests were performed to assess the retained strength of impact-damaged plates. Three test series were run to evaluate the effect of various cross-ply and angle-ply arrangements. A fourth series on $[0°_5/90°_5/0°_5]$ glass/epoxy plates showed linear dependences of both retained strength and retained stiffness on delaminated area, although stiffness decrease was much less than strength decrease. Some tests with simulated delaminations (by mylar sheet inserts of the same area) correlated closely with tests of damaged plates, indicating that the strength decrease was attributable to delamination and not to other damage mechanisms. Exploratory tests were made with other material systems (graphite/epoxy and Kevlar/epoxy). Stacking sequence effects in the graphite/epoxy plates were strikingly different from the effects in glass/epoxy, illustrating the hazards of trying to predict the behavior of one system from observations on another system.

TABLE OF CONTENTS

LIST OF FIGURES

LIST OF TABLES

SECTION I

INTRODUCTION

The subjects discussed in this final technical report represent selected areas of research conducted under Grant number DAAG29-79-G-0007 which have not been reported in prior publications or technical reports. The overall program has focused attention on the ability of structural elements to withstand short duration transient loadings in which the stress and deformation are transmitted through the material. The prediction and control of the generated failure zones in material systems subjected to transient loadings requires basic information on the dynamic material properties and the mechanisms by which the stress and deformation propagate through the material. It is recognized that these problems are interrelated, since the dynamic material properties must be determined experimentally under conditions of transient loading where the stress and deformation are not uniform through the test specimen, and of course the stress wave propagation, dispersion and attenuation depend upon the dynamic properties. In the present program the response of a representative class of continuous filament composite materials subjected to central impact loadings on plate type structural elements has been examined. The effects of varying the impactor nose shape, mass, and length as well as considering geometric variations in the lamina stacking sequence of the composite plate specimens have been discussed in previous reports and publications. Effects examined include energy absorption, delamination crack propagation, transverse cracks, and flexural wave propagation.

Those topics investigated but not previously fully documented through formal reporting procedures have been included in this report. Three specific program areas are described: (1) the development of a multi-channel transient recording system, (2) the analytical prediction of the interlaminar shear stresses in the elastic flexural wave and estimates of the threshold levels of shear stress for interlaminar shear failure through use of appropriate computer codes, and (3) experimental residual strength and stiffness studies of damaged plates subjected to transient loads. Each of these topics is discussed separately in the succeeding sections. Results and conclusions are given separately in each of these sections.

SECTION II

TRANSIENT RECORDING SYSTEM

(a) Introduction

In the research on the transient deformation following ballistic impact on a laminated composite structural element it was desired to record strain and other information simultaneously from a number of locations on the same specimen following a single impact. The difficulty of accomplishing this is related first to the speed of the event and the number of channels of information to be recorded, and secondarily to the cost of instrumentation which will satisfy these requirements. In the case of fiber reinforced laminated panels the total duration of the transient events of interest ranges from 0.1 to 10 milliseconds with rise times on the early features of the signals in the neighborhood of 1 to 10 microseconds. Concerning an optimum number of channels for signal recording, an exact number cannot be given but 8 should be a reasonable minimum and 16 should be practical in many applications. The larger the sample, the larger the number of sensors that are reasonable and then cost becomes the major determining factor, if instrumentation is available.

The first practical approach to recording high-speed transient signals was to use a camera to photograph the display of a cathode ray oscilloscope. This approach provides the necessary speed but has limited resolution and normally only 2 (at most 4) channels. It results in a single photograph, from which it is not easy to obtain quantitative results for comparison with numerical models, etc. To obtain quantitative high-resolution data from these transient signals one would like to sample and digitize each of them at a sufficiently high rate so that none of the information is lost. This requires sample rates of 1 to 10 MHz for each signal. If electronic digitization of the signal is to be accomplished in real time very high speed analog-to-digital converters are required for each signal channel, and digital memory devices fast enough to store the information are required. The first electronic transient recorders which use this approach and sample the signals at > 1 megahertz were designed in the early 1970's. Such equipment works well but is relatively expensive. The best known manufacturer of this type of transient recorder in the U.S. is Gould-Biomation. Another approach to sampling and digitizing transient waveform information became feasible

starting in about 1978. A newly developed electronic device called the charge coupled analog shift register or CCD register provided a means to sample and temporarily store the transient signal in analog form. With this device it became possible to develop a process analogous to "slow motion" photography, wherein the transient signals are sampled at the necessary rate and temporarily stored in CCD registers until they are read out at much slower rates to the fewer and less expensive analog-to-digital converters and memory devices required. Either type of electonic transient recorder can be interfaced to a digtal computer so that the transient waveform information can be printed, plotted, or otherwise analyzed.

(b) Development of a Transient Recorder using CCD Registers

In the summer of 1978 a family of CCD devices was announced by Reticon Corporation of Sunnyvale, California. One product in this family, a Type R5103 video analog delay device, seemed particularly appropriate for use in developing a design for a transient recorder system. Because this was a sole source device its specifications were examined very carefully in printed form and then in several telephone discussions with engineers at Reticon Corporation. All indications were that the device was apropriate for this application. The development of a transient recorder based on this device was then included in a research proposal and received approval. The initial objective was to build an 8 channel recording system with a sample rate capabilty of at least 1 MHz per channel. In the first half of 1979, 2 Type R5103 CCD devices were acquired and tested in a breadboard circuit to gain information necessary for circuit design of the transient recorder. Components for the recorder were then ordered, including 14 additional Type R5103 CCD devices. In the fall of 1979 actual circuits designed for the recorder were breadboarded and tested thoroughly before developing printed circuit cards for the recorder circuitry. At this point it was noticed that the R5103 devices were not meeting their published specifications in one crucial property. The leakage rate for charge packets stored in the device was much higher than was specified. This finding was documented well and submitted to the engineers at Reticon. It was admitted by Reticon that their specification was in error, and the Reticon engineers suggested that a newer device not yet announced for marketing was much improved in this respect and should meet the requirement for the transient recorder. Samples of the newer device, an R5104, were supplied by Reticon in February of 1980. Tests at the

University of Florida confirmed that the leakage of the R5104 is much less than that of the R5103. However, in order to achieve the improved performance, the architecture of the newer device has been changed significantly from that of the R5103, and in order to use the newer device much of the circuitry of the transient recorder would have to be redesigned. Although both devices are dual shift registers (i.e. two registers in one package) and one set of clock signals drives both registers in a package, the R5103 samples the input signal in an alternating sequence for the two shift registers whereas the R5104 samples the signals at its inputs simultaneously into its two registers. The architecture of the R5103 is much better for the design of a transient recorder than that of the R5104, but its leakage is much worse.* In July 1980, the decision was made to use the R5104 device. Reticon exchanged the R5103s for the newer R5104s.

During 1981 the transient recorder was redesigned and has been constructed and tested. The system is an 8 channel system which functions at sample rates up to 5 MHz per channel and includes pretrigger recording capability. It is interfaced to a microprocessor system with a dual floppy disk memory, a video terminal, and a printer. Transient waveform records can be stored on a floppy disk, printed, or both. The ability to plot the recorded waveforms or transfer data sets to other computers can be added.

(c) A Brief Description of the Transient Recorder Design

The design of the transient recorder is outlined in the block diagram of Figure 1. The preamplifiers are d.c. coupled 2 MHz bandwidth amplifiers with differential inputs. They are designed for use with strain gages and bridge type transducers as well as voltage input signals. Output signals from the preamplifier channels are connected to inputs of CCD shift register channels which (under the control of the read-in and read-out control logic) sample, store, and later read out 590 analog samples for each input channel. The read-in control logic provides means to select with external controls the sample rate and the number of pretrigger samples to be retained and to enable and trigger the system to record a transient event. It also maintains the synchronization of the system while sampled data is being loaded into the CCD

*Device specification available from EG&G Reticon Corp., 345 Portrero Ave., Sunnyvale, CA 94086

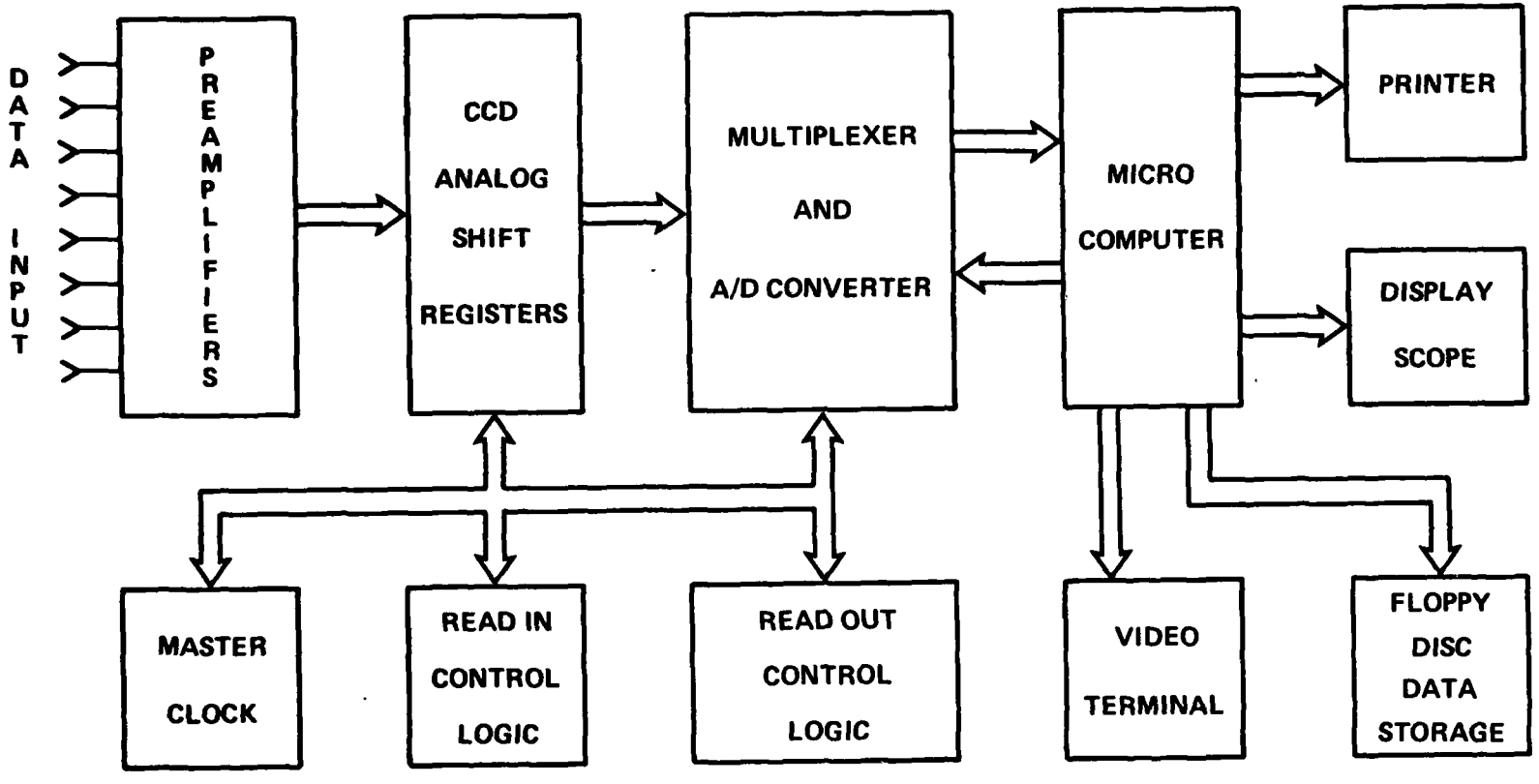

Figure 1. Block Diagram of The Present Transient Recorder System

registers and transfers control to the read-out control logic when the CCD registers are fully loaded. Samples are taken into each of the CCD register channels simultaneously during the read-in (data acquisition) period but the CCD registers must be unloaded sequentially. The read out control logic maintains the synchronization and does the "bookkeeping" necessary to unload the analog samples from the CCD registers through the multiplexer and analog to digital converter, enter the digital sample values into the microcomputer, and bring the system to an orderly halt when finished. All of the control logic is constructed with standard TTL logic. The microcomputer uses a Motorola Type 6809 processor and is programmed to accept the digital data, format it and create floppy disk storage files, and then enter an interactive program which offers the operator several standard routines to print, plot, or display the data.

(d) Tests of the Transient Recorder

I. Tests with known input waveforms from signal generators

To demonstrate the fidelity of the transient recorder, waveforms from signal generators were recorded, and the records were compared to the known input waveforms. An example of such a test is one in which 2 cycles of a triangular waveform at 20 μsec per cycle were recorded. First the input waveform was recorded on a digital oscilloscope at a 2 MHz sample rate and plotted on an X-Y plotter. Next the waveform at the input of the A/D converter within the transient recorder after being sampled and time stretched was recorded on the digital oscilloscope and X-Y plotted. Finally the numerical data from the digitized record was stored in the microprocessor and printed. It was possible to test each of the 8 channels in the system in this way. The results of this test for one channel are shown in Figure 2. The step-like structure of the trace in Fig. 2a. is caused by the digital oscilloscope sampling, and is not present in the actual signal recorded. Conclusions from such tests are: (1) the transient recorder does perform its intended function, (2) the level of noise which is mixed with the signal within the transient recorder is noticeable and needs to be reduced, and (3) the baseline slope at the output of the CCD device needs to be eliminated. Both the noise and slope can be treated with hardware modifications.

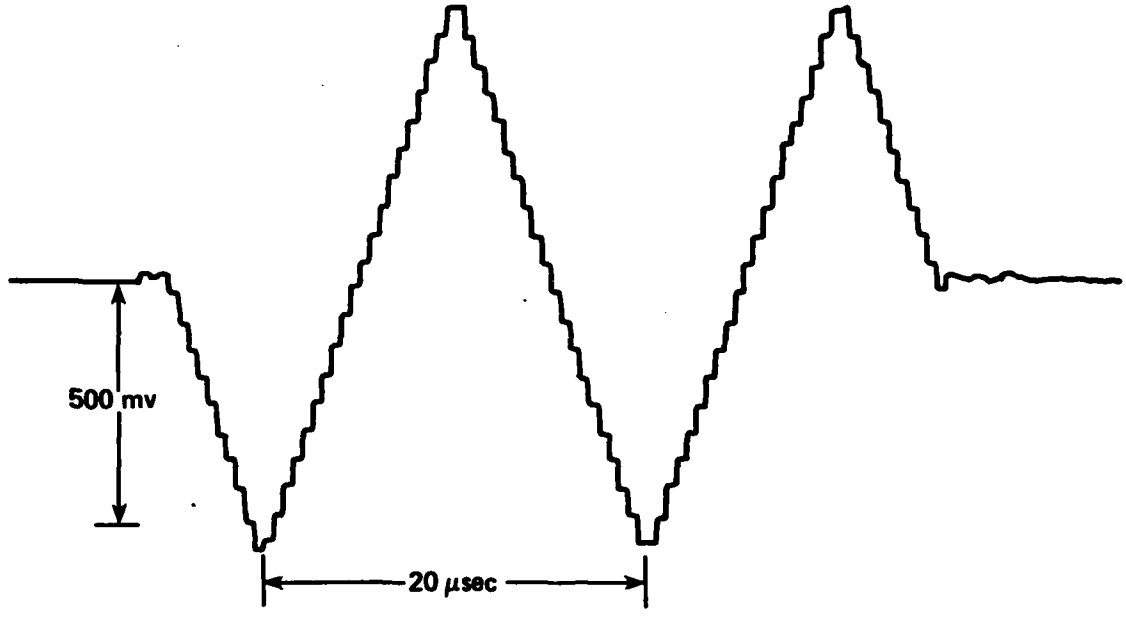

Figure 2A. Triangular Waveform Test Signal From a Signal Generator as Recorded by a Digital Oscilloscope at a 2 MHz Sample Rate And Later XY Plotted.

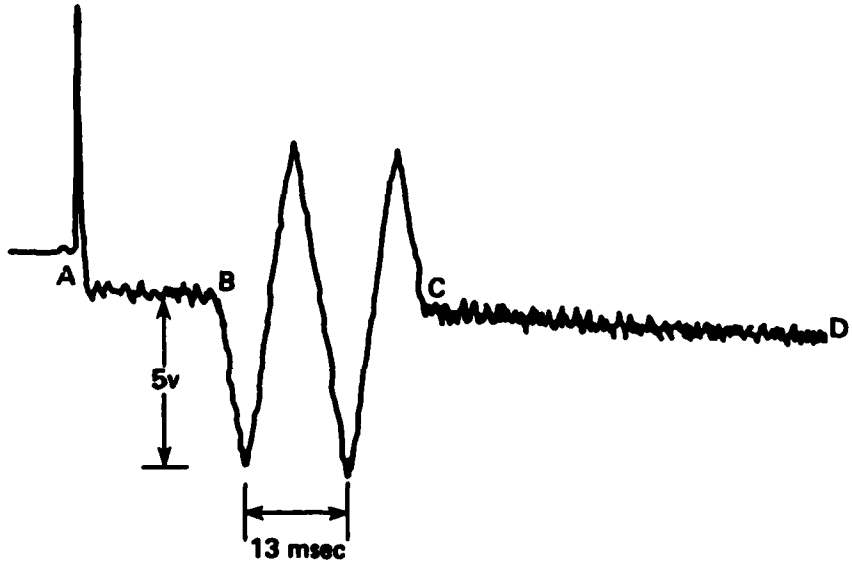

Figure 2B. Test Signal After Time Stretching by The Transient Recorder CCD Registers.

II. Tests using strain gages on a laminated plate

A second series of tests has been performed to evaluate the recording system's performance in its intended application. The transient strain waveforms from a laminated plate with gages at 8 locations were captured, digitized, recorded on a floppy disk, and printed in tabular form. As a part of the testing procedure, at the front end CCD register part of the system, input and output waveforms of 2 channels were recorded on digital oscilloscopes during the actual tests. Two laminated plates with 8 gages each have been tested and each plate has been subjected to more than one impact. Results from tests on one of these panels are displayed in Figures 3A and 3B. The programming to plot the waveforms from the digitized data set has not yet been completed but that is a relatively straightforward task. No unexpected performance characteristics have been observed in the second series of tests.

(e) Current Status of the Transient Recorder System

The recording system is functional at the present time. Work is being done to minimize the problems with baseline slope and with internal noise that were noticed in the first series of tests. A means to examine and plot the waveforms from the recorded data sets is also being implemented. It is expected that this system will serve in this laboratory for a number of years. There is, however, less optimism about the use of CCD analog registers in the design of transient recorder systems than four years ago because one of the objectives in developing a system designed with CCD devices was to achieve good performance at relatively low system cost. It appears now that market forces in the electronics industry are motivating rapid improvements in high-speed low-cost integrated analog-to-digital converters and high-speed memory devices while CCD analog shift registers are receiving significantly less attention because they have a lower volume market, and therefore it is likely that direct analog-to-digital conversion may emerge as the better design approach for sampling rates in the 1 to 10 MHz range. At sample rates of 10 to 100 MHz CCD analog registers are still in principle very attractive, but appropriate integrated circuit devices are not generally available to designers. By developing in-house a custom CCD device, Phillips Test and Measuring Instruments (Mahwah, N.J.) has recently designed and marketed a

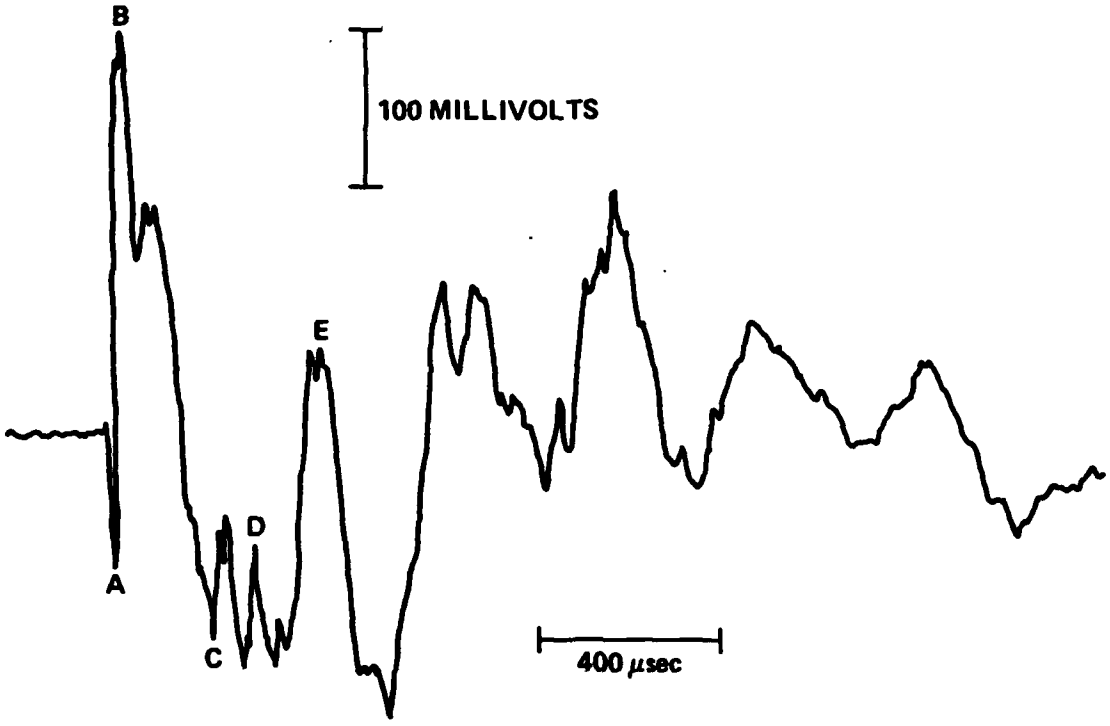

Figure 3A. Actual Strain Waveform From a Gage On a Laminated Plate. This Waveform Was Recorded By a Digital Oscilloscope Connected To The Input of The Transient Recorder.

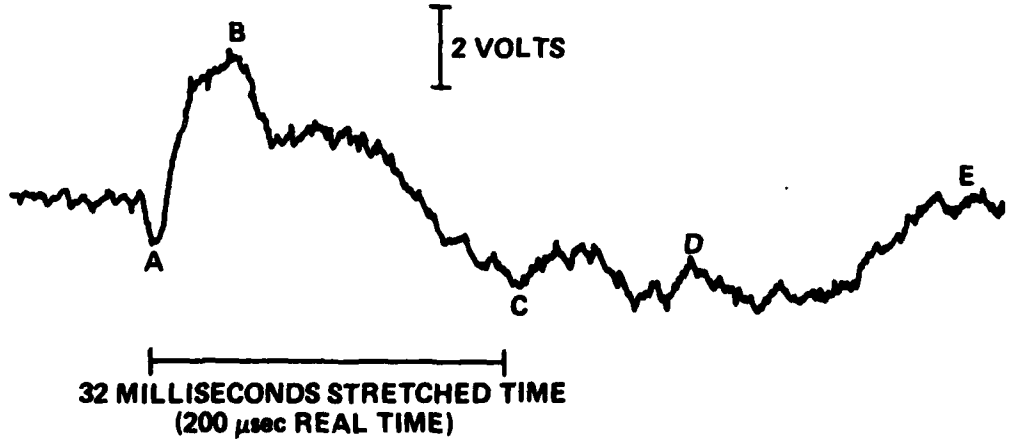

Figure 3B. The Same Strain Waveform as Shown in Figure 3A After Time Stretching by The Transient Recorder CCD Registers. Several Corresponding Features Have Been Labeled in Both Figures.

digital storage oscilloscope (model PM3310) with a maximum sampling rate of 50 MHz.

In conclusion, multichannel transient recorder systems including the necessary preamplifier systems and computer hardware are not destined to become inexpensive but should become relatively less expensive and more available to research groups than in the past.

SECTION III
FINITE ELEMENT ANALYSIS OF INTERLAMINAR SHEAR STRESS

(a) Introduction

In an effort to determine analytically the interlaminar shear stress of a crossplied fibrous composite subjected to a localized low velocity impact two analyses were used. The first method was accomplished using a computer program for Dynamic Elastic Plastic Response Of Panels [DEPROP, (Ref. 1)]. DEPROP is a computer program using finite-strain plate theory, a bilinear elastic-plastic material and a von Mises yield criterion for metals. In addition it will handle an elastic multilayered orthotropic material, but because the plate theory in the code does not include shear deformation effects, the transverse shear stress is not calculated directly by the program. Transverse shear stresses were therefore calculated by integrating the stress equations of motion, using the bending normal stress gradient through the thickness determined from the DEPROP calculation as input and assuming that the in-plane acceleration component was negligible. This procedure appeared to give reasonable results but was too cumbersome and laborious. Results of this study were given in Reference 2 both as tabulated values of τ_{xz} versus time at an interface of a three-lamina plate at a point 1.22 cm from the center of the plate on the line of symmetry where τ_{yz} is zero, and also as a plot of τ_{xz} versus z, the coordinate in the thickness direction at the same point.

More recently a structural analysis finite element computer program, SAPIV (Ref. 3), was acquired. This program has a three dimensional elastic orthotropic material analysis capability which calculates the transverse shear stress directly. This program was used to calculate the interlaminar shear stress of a $[0°_5/90°_5/0°_5]$ glass/epoxy plate when subjected to center point impact of 45.7 m/sec (150 ft/sec) by a cylindrical steel projectile of 0.97 cm diameter and 2.54 cm in length. The following sections describe this analysis.

(b) Model

Because of the symmetry of loading, only one quarter of the plate was analyzed. The lines of symmetry and conditions for ensuring symmetry of the

solution are shown in Figure 4. The plate was analyzed using three dimensional eight node elements shown schematically in Figure 5. The fiber directions are in the x-direction for the top and bottom laminas, and in the y direction for the middle lamina. The cell size near the lines of symmetry was chosen as 0.25 x 0.25 x 0.0625 in (0.635 x 0.635 x 0.159 cm). At other points the size was 0.5 x 0.5 x 0.0625 in (1.27 x 1.27 x 0.159 cm). Nodes were assigned along the lines of symmetry, which means that the center of the closest elements to the lines of symmetry was 0.125 in (0.318 cm) from the lines of symmetry.

The stress output for the program is at the center of each element and at the center of each face of the element. The interlaminar shear stresses shown in the results section were obtained by taking the average between the lower surface of the top element and the upper surface of the middle element, and the average between the lower surface of the middle element and the upper surface of the bottom element. Thus interlaminar shear stresses were not calculated on the lines of symmetry of the plate. The plotted results are always at least 0.125 in from a symmetry line.

The solution is a displacement type with three translational degrees of freedom at each node. In order to ensure no rotations about lines along and normal to the fixed sides and lines of symmetry, zero rotation boundary elements were used at these places.

(c) Material Properties

The constitutive relations of the material used for the plate are written in terms of the global axes x, y, z shown in Figure 5. These equations as given in the SAPIV manual (Ref. 3) are

$$
\begin{aligned}
\varepsilon_x &= (1/E_x)\sigma_x - (\nu_{xy}/E_y)\sigma_y - (\nu_{xz}/E_z)\sigma_z \\
\varepsilon_y &= -(\nu_{yx}/E_x)\sigma_x + (1/E_y)\sigma_y - (\nu_{yz}/E_z)\sigma_z \\
\varepsilon_z &= -(\nu_{zx}/E_x)\sigma_x - (\nu_{zy}/E_y)\sigma_y - (1/E_z)\sigma_z \\
\gamma_{xy} &= \tau_{xy}/G_{xy}, \qquad \gamma_{yz} = \tau_{yz}/G_{yz}, \qquad \gamma_{zx} = \tau_{zy}/G_{zy}
\end{aligned}
\tag{1}
$$

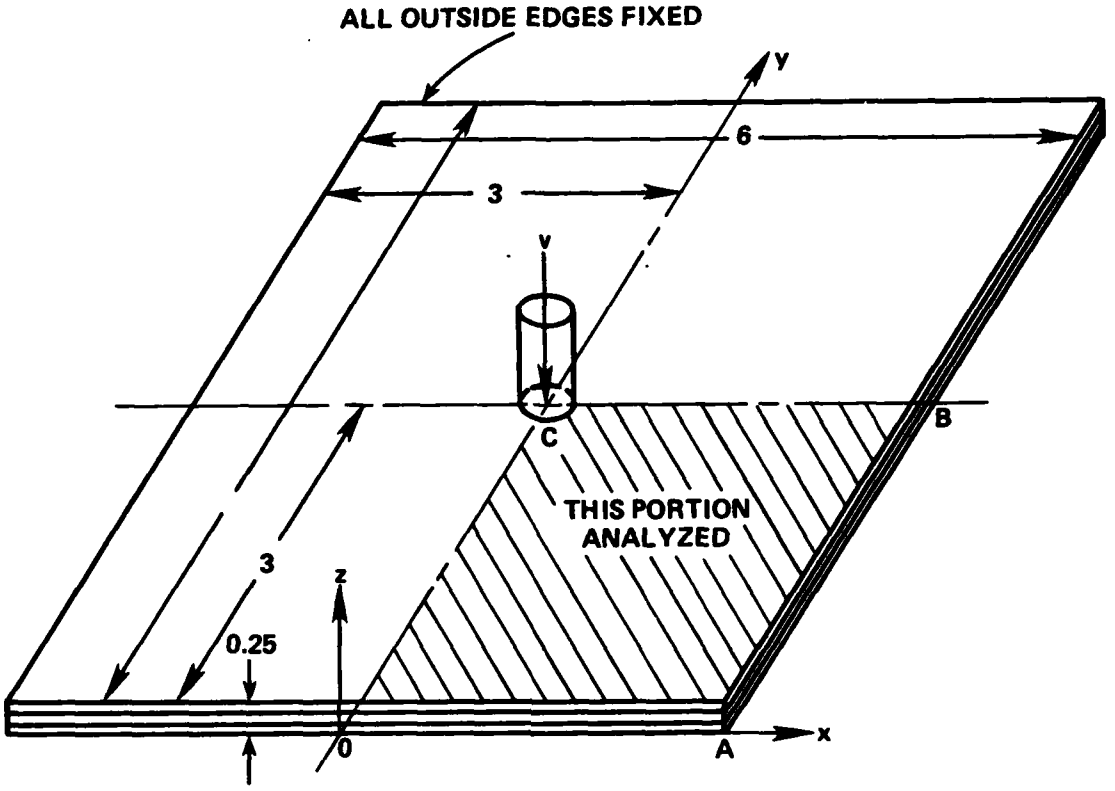

BOUNDARY CONDITIONS

Line or Point	Condition
0A	All rotations and displacements are zero
AB	All rotations and displacements are zero
0C	Rotations about 0C and all displacements in x direction are zero
BC	Rotations about BC and all displacements in y direction are zero
C	All rotations and displacements, except displacement in z direction, are zero

Figure 4. Loaded Plate Showing Lines of Symmetry. All Dimensions in Inches.

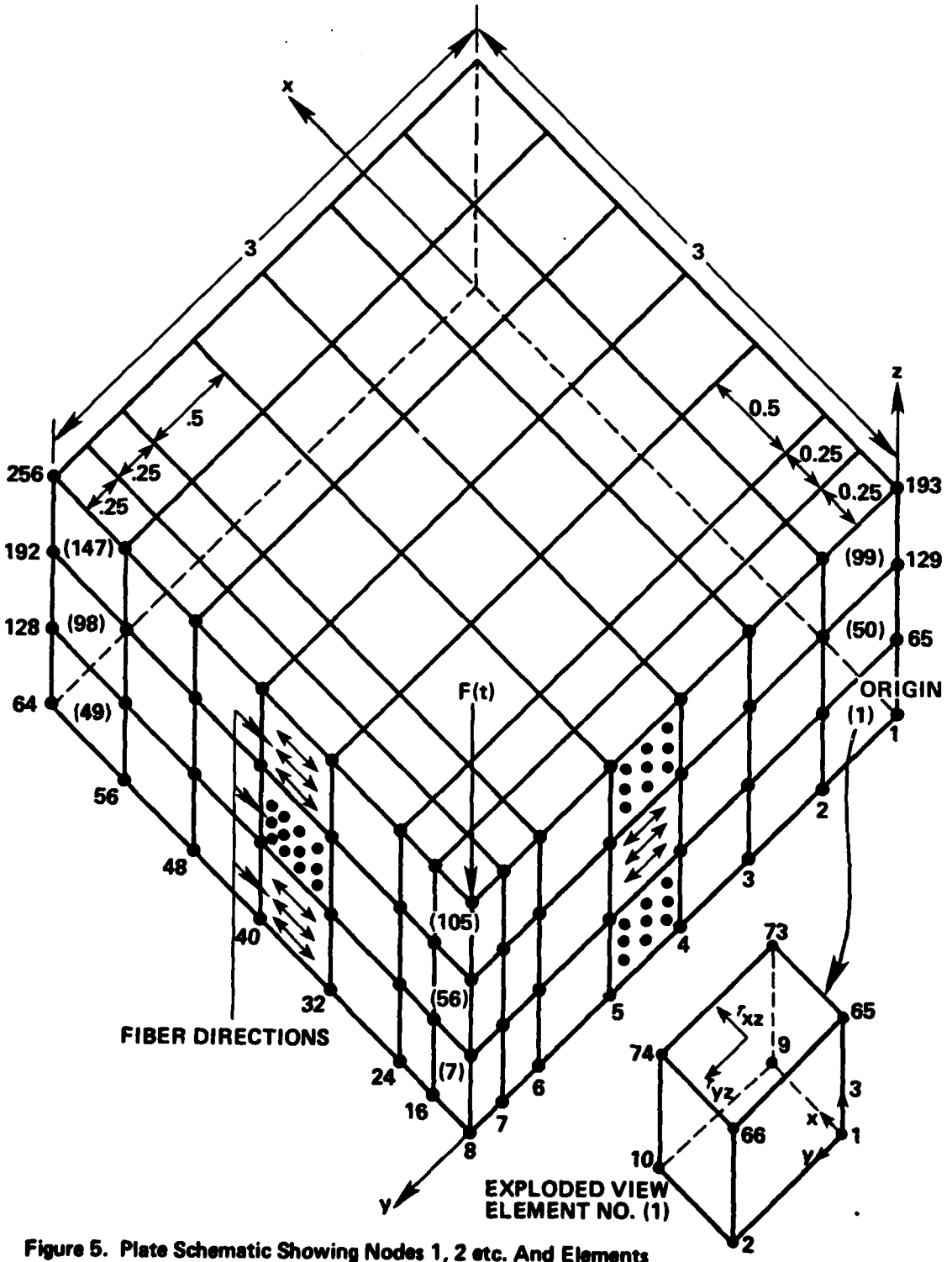

Figure 5. Plate Schematic Showing Nodes 1, 2 etc. And Elements (1), (2) etc. Drawing Not to Scale Node No. 8 is Bottom Center Point. Load is Applied at Node No. 200, Top Center Point.

where

ε = unit extension, dimensionless

γ = shear strain, dimensionless

σ = normal stress, psi

τ = shear stress, psi

E = modulus of elasticity, psi

ν = Poisson's ratio, dimensionless

G = shear modulus, psi.

The top and bottom laminas with the fibers aligned in the x direction (0°) have elastic properties of Material 1. In the middle lamina the fibers are aligned along the y direction (90°) and have elastic properties given as Material 2. The elastic properties of these two materials are given in Table 1.

TABLE 1

MATERIAL PROPERTIES

Elastic Property	Material 1	Material 2
E_x, 10^6psi	5.80	1.20
E_y, 10^6psi	1.20	5.80
E_z, 10^6psi	1.20	1.20
ν_{xy}	0.05	0.24
ν_{xz}	0.05	0.30
ν_{yz}	0.30	0.05
G_{xy}, 10^6psi	0.60	0.60
G_{yz}, 10^6psi	0.44	0.60
G_{xz}, 10^6psi	0.60	0.44

(d) Loading Function

The loading-time function was determined from the mass of the projectile and the contact time of the projectile and the plate. The weight of the projectile was 0.031 lbs. and the contact time for impact of v_o = 150 ft/sec was 0.25 millisec. A linearly varying force-time relationship was assumed as shown in Figure 6. The impulse magnitude I is the area under the force-time curve and may be expressed as

$$I = \frac{F_{max}(\Delta t)}{2} = |\Delta(mv)| = mv_o \qquad (2)$$

where $|\Delta(mv)|$ is the magnitude of the change in momentum of the projectile and Δt is the contact time of the projectile on the plate. Thus

$$F_{max} = 2\frac{(mv_o)}{\Delta t}, \qquad (3)$$

and for the 150 ft/sec impact

$$F_{max} = \frac{2(150)(.031)}{(32.2)(.00025)} \simeq 1200 \text{ lbs}$$

gives an impulse approximately equal to that imparted by the projectile. One-fourth of this is assumed to be transmitted to each quadrant of the centrally impacted plate. Thus the loading at the point C (Figure 4) for the quarter plate is initially 300 lbs and decays linearly to zero in 0.25 millisec.

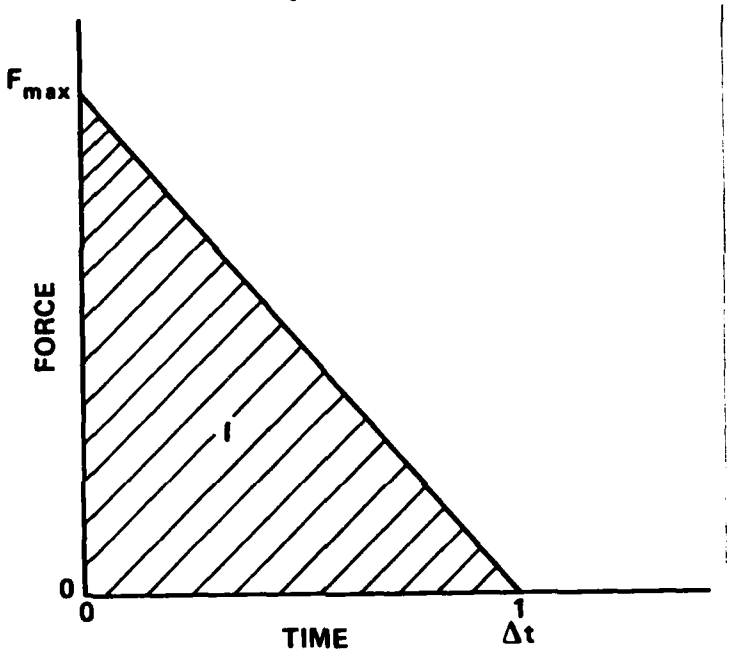

Figure 6. Assumed Force–Time Relationship.

(e) Results and Discussion

Based on the above discussion, the SAPIV program was exercised for the 150 ft/sec impact. Interlaminar shear stresses for both the top and bottom interlaminar planes were determined and are shown in Figures 7-11. The top interlaminar plane is the one closest to the impact side and the bottom interlaminar plane is the one farthest from the impact side. The signs of the shear stresses are shown in positive direction on the top of element No. 1 of Figure 5.

The lower right part of each figure shows the locations of the stations, A through G, for which interlaminar shear stress histories are shown in the plotted curves. Ordinate scales are ksi. It is seen in Figures 7 and 8 that

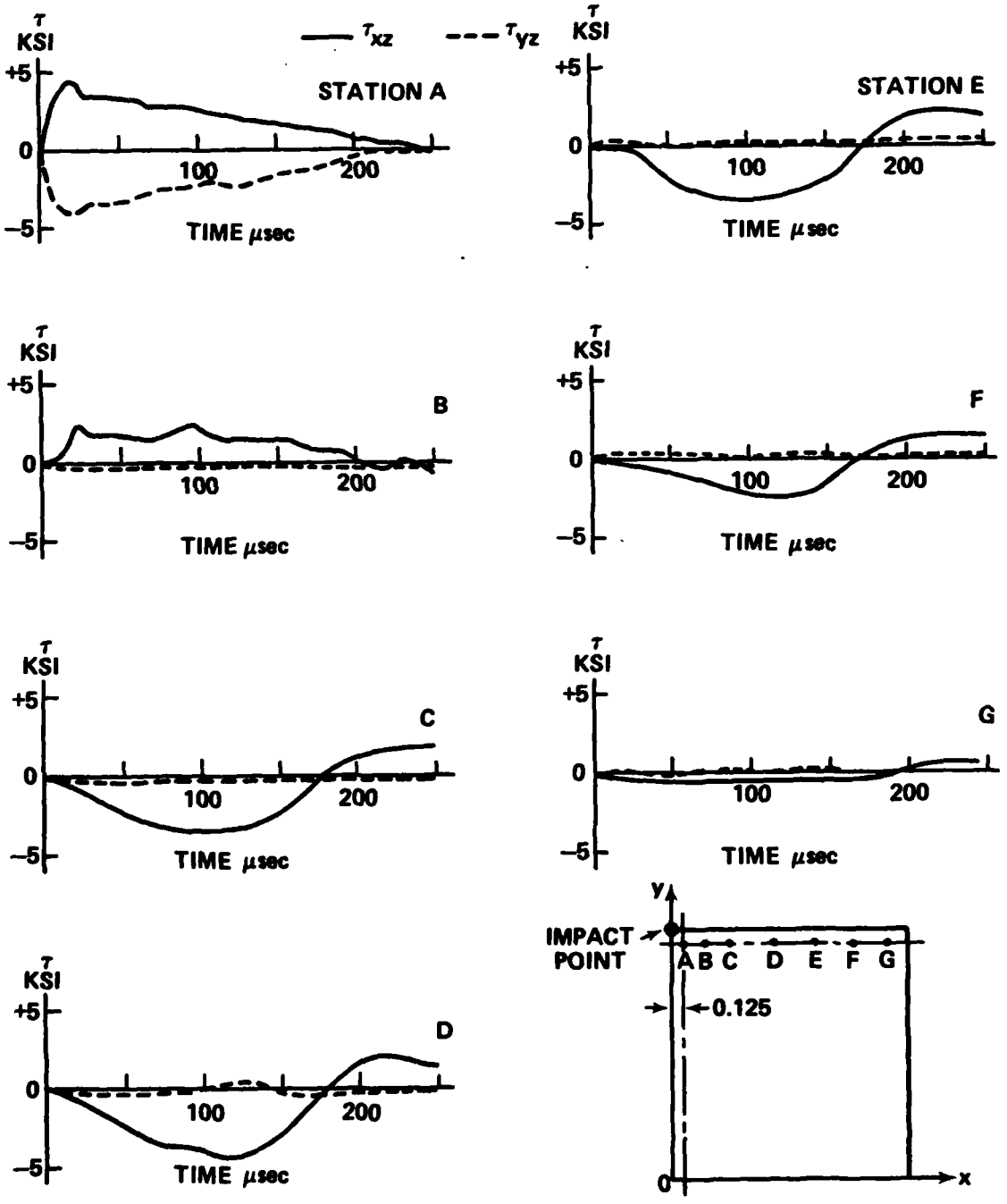

POINT	A	B	C	D	E	F	G
x DISTANCE FROM IMPACT POINT (IN.)	0.125	0.38	0.75	1.25	1.75	2.25	2.75

Figure 7. Shear τ_{xz}, τ_{yz}, Top Interlaminar Plane Vs. Time. Stresses For Stations A to G Parallel to x Axis.

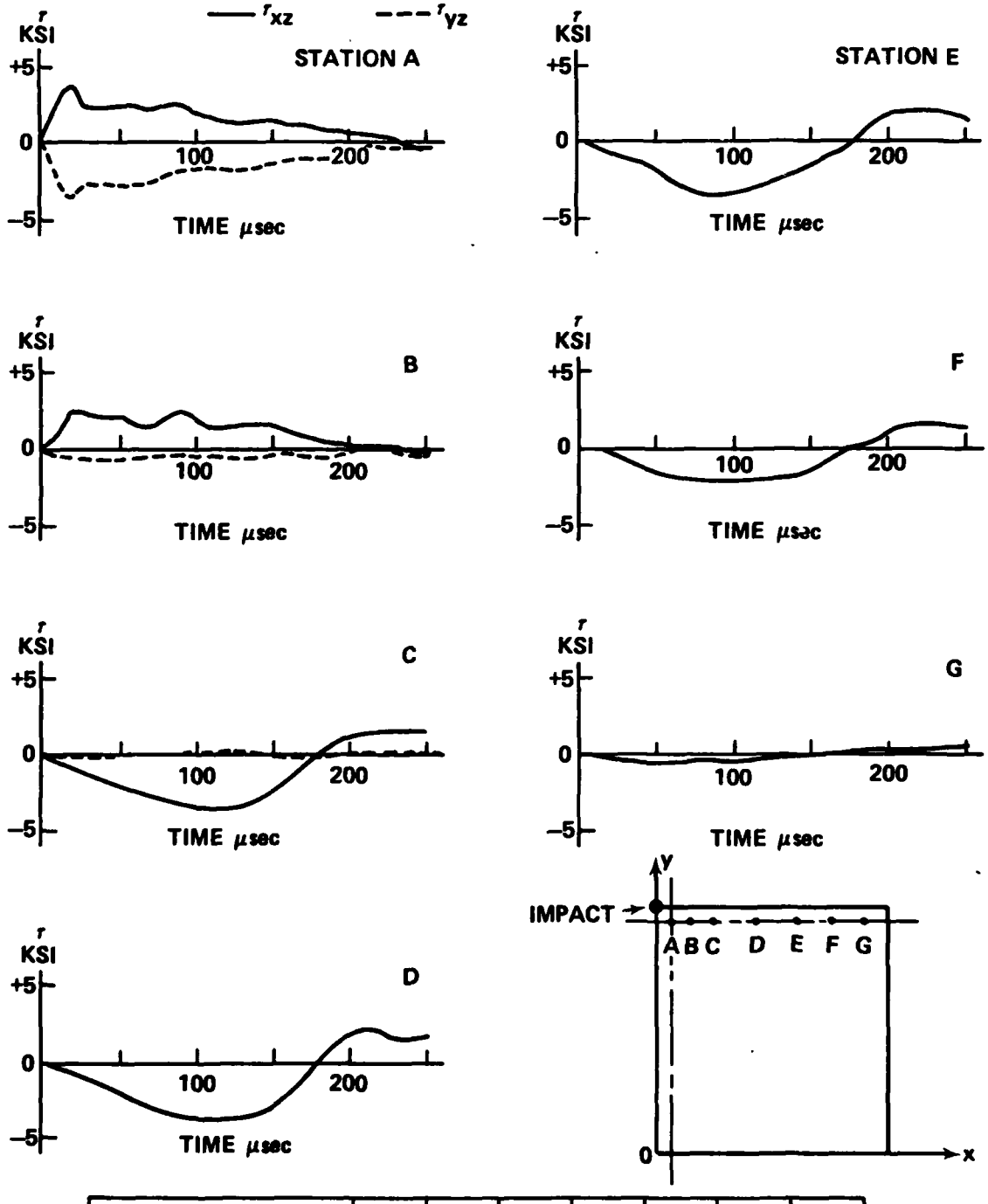

POINT	A	B	C	D	E	F	G
x DISTANCE FROM IMPACT POINT (IN.)	0.125	0.38	0.75	1.25	1.75	2.25	2.75

Figure 8. Shear Stress τ_{xz}, τ_{yz}, Bottom Interlaminar Plane Vs. Time. Stresses For Stations A to G Parallel to x Axis.

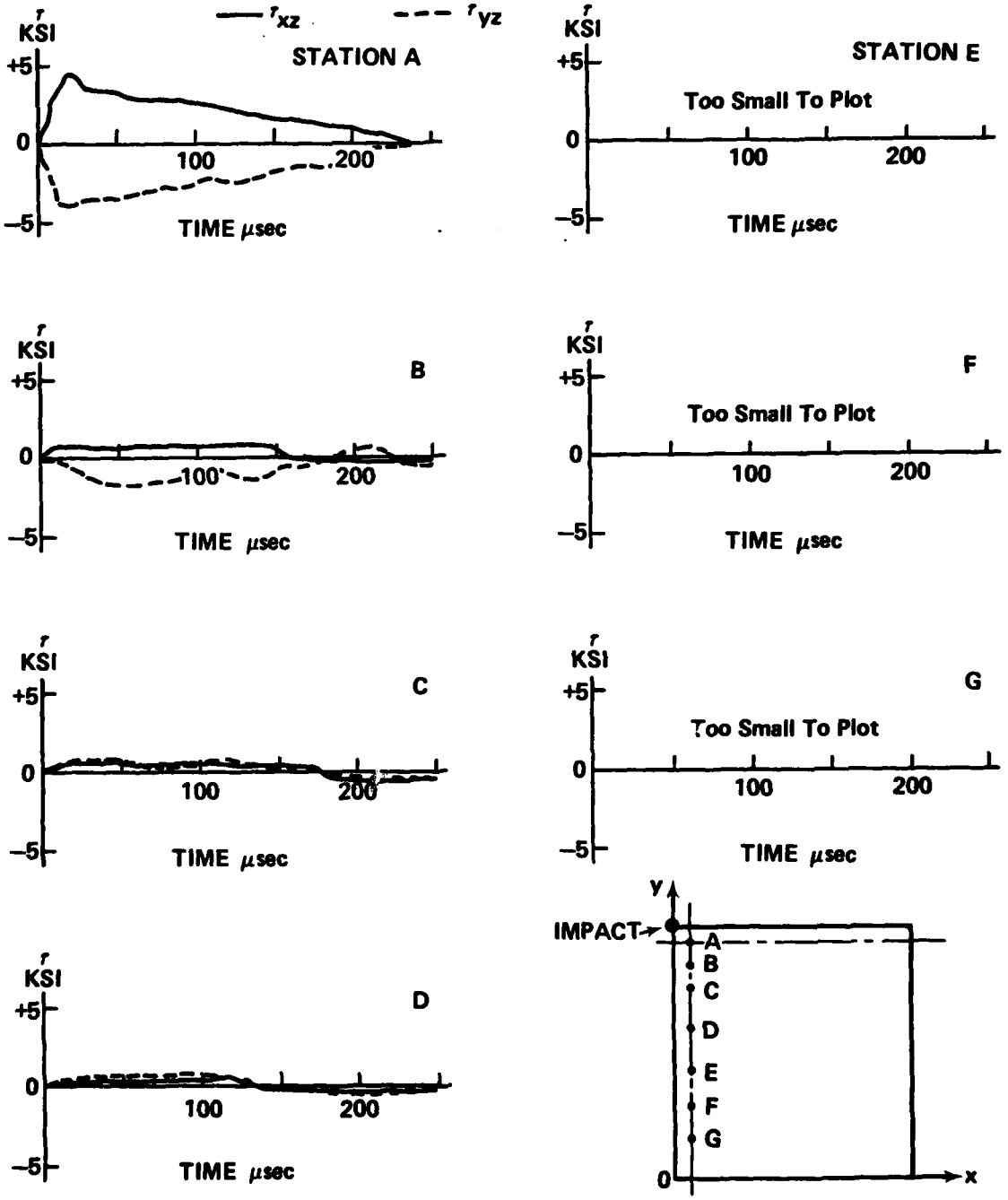

POINT	A	B	C	D	E	F	G
y DISTANCE FROM IMPACT POINT (IN.)	0.125	0.38	0.75	1.25	1.75	2.25	2.75

ure 9. Shear Stress τ_{xz}, τ_{yz}, Top Interlaminar Plane Vs. Time. Stresses For Stations A to G Parallel to y Axis.

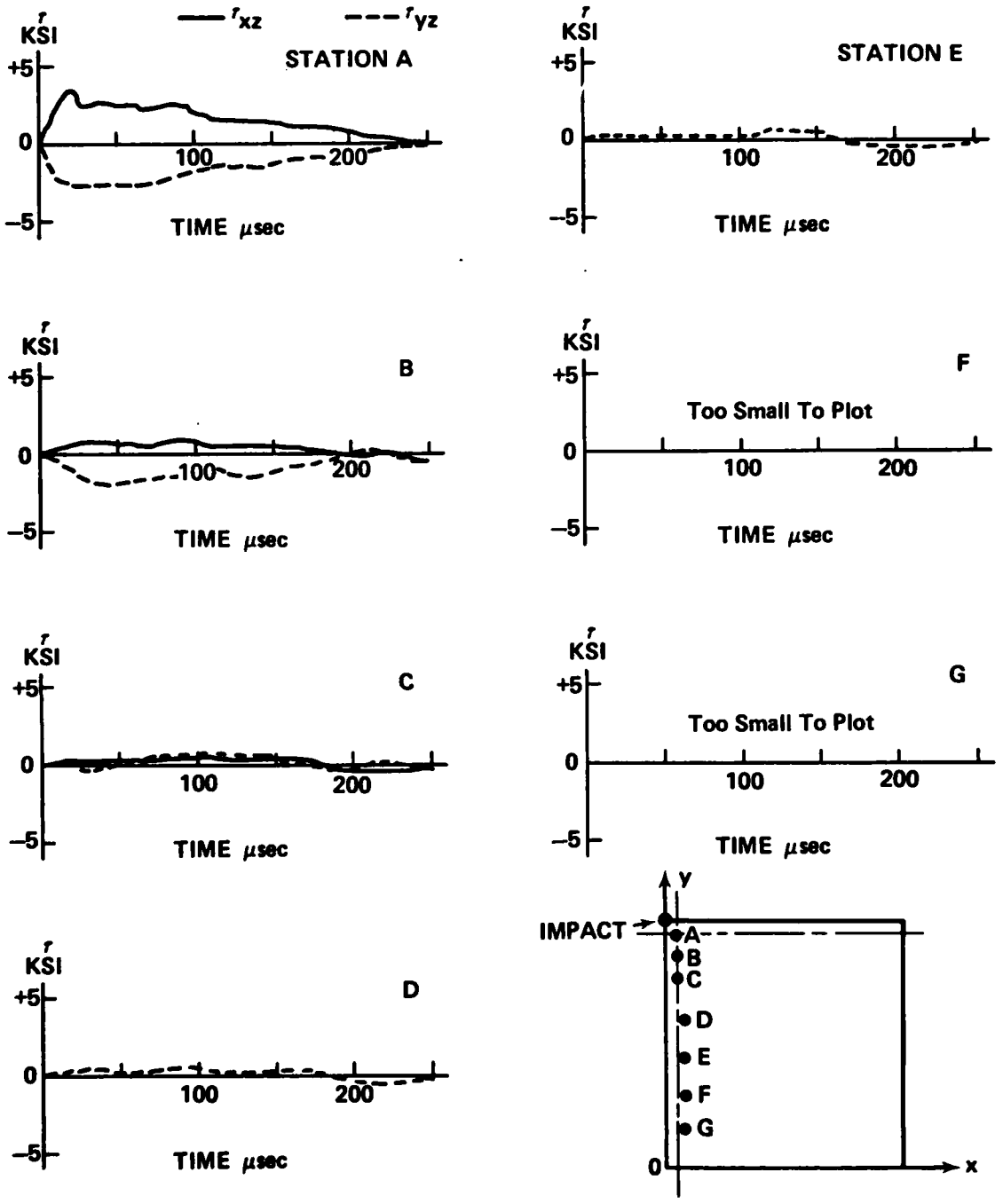

POINT	A	B	C	D	E	F	G
y DISTANCE FROM IMPACT POINT (IN.)	0.125	0.38	0.75	1.25	1.75	2.25	2.75

Figure 10. Shear Stress τ_{xz}, τ_{yz}, Bottom Interlaminar Plane Vs. Time. Stresses For Stations A to G Parallel to y Axis.

according to the elastic solution the shear stress τ_{xz} attains or exceeds the estimated interlaminar shear strength of 2.5 ksi at almost every station along the line parallel to the x-axis (fiber direction of the top and bottom laminas) in both interlaminar planes. The shear stress τ_{yz} is much smaller along this line, which is near the symmetry plane where $\tau_{yz} = 0$, except at Station A near the impact point. Station A is at the same distance from the two symmetry planes, and the two shear stress components at Station A are approximately equal in magnitude there, as would be expected. From Figures 9 and 10 the calculated shear stress along the line at 90° to the top and bottom fiber direction exceeds the interlaminar shear strength only locally near the impact point. Experimental studies of the impact simulated by this calculation [Refs. (1) and (2)] show that in the bottom interlaminar plane the delamination extends about half way to the boundary in the 0° direction parallel to the fibers of the bottom lamina while the delamination in the 90° direction extends approximately half as far as that in the 0° direction. The difference between experiment and calculation is even greater in the top lamina, where the experiment actually shows delamination extending at least as far in the 90° direction as in the 0° direction. The top interlaminar plane has less delamination than the bottom one in the experiment, while the elastic solution of Figures 7 to 10 indicates aproximately the same interlaminar shear stresses in the two interlaminar planes. The different delamination behaviors in the two planes is attributed to the sequential delamination mechanism, initiated by a generator strip in the top lamina as described in Refs. 4-7. When actual delamination cracks begin to propagate the elastic stress field would be considerably changed.

The spatial distribution parallel to the x axis for the shear stress τ_{xz} of the top interlaminar plane is shown in Figure 11 for various times. This curve (Figure 11) was generated as a crossplot of the data of Figure 7. The plots of Figure 11 show that the shear stress τ_{xz} changes sign at about x = 0.5 in. It is remarkable that this distance is essentially the same in all the plots. At 110 microseconds the negative shear stress magnitude exceeds 2.5 ksi almost all the way to the boundary. These results are all based on elastic response and take no account of the delamination which would occur at these stress levels and which would modify the actual shear stress distributions as the delamination crack propagates.

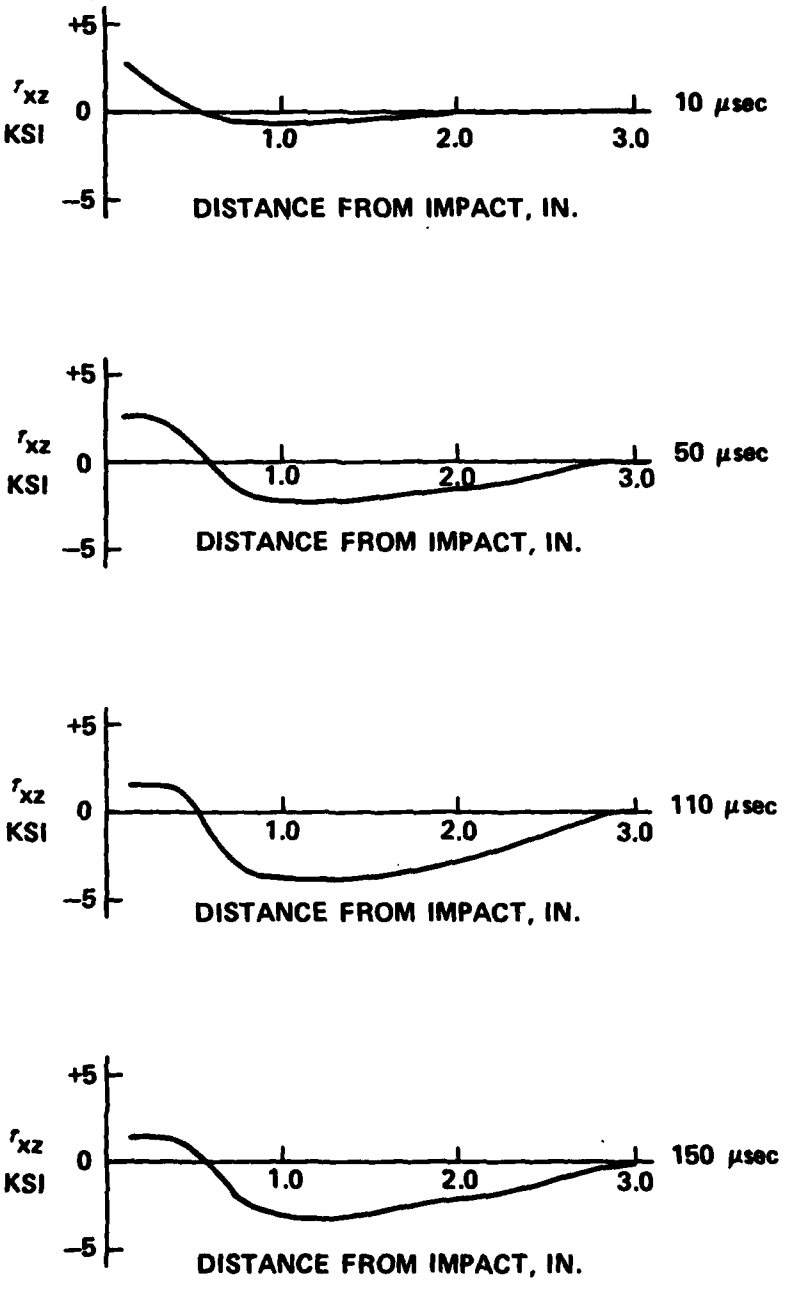

Figure 11. Shear Stress τ_{xz} Vs. x Distance From Impact Point For Given Times Shown On Right Hand Side.

SECTION IV
RESIDUAL STRENGTH STUDIES

(a) Introduction

Previous investigations in this program have shown that in laminated plates formed from unidirectionally reinforced laminas of continuous glass fibers in an epoxy matrix the energy absorption in impacts by small steel cylindrical impactors at subperforation speeds is a linear function of the total delaminated area (Refs. 4-7). An important problem remains, however, namely the effect of the damage sustained in stopping the impactor on the usefulness of the damaged plate as a structural element.

Retained strength after impact could be characterized in several different ways. Tests could be made in tension, compression or bending, for example, either in monotonic or cyclic loading. Different types of tests might produce different results. The choice of test could be guided by the particular function that the damaged element was expected to perform.

For the preliminary investigation reported here, static three-point cylindrical bending tests were performed in which the square plate, supported on two edges, was centrally loaded by a wedge with a rounded edge. This type of test had the advantage that it was easy to perform, gave a clearly identifiable point of maximum load and proved to be surprisingly reproducible.

All the tests of damaged plates were made on the full-size 15.24 x 15.24 cm (6 x 6 in.) plates that had been previously impacted at various speeds by blunt-ended steel cylinders, producing various amounts of delaminated area. The tests measured the residual strength of the whole structural element rather than the local strength and stiffness of the damaged region. The results obtained were therefore particular to the size of plate employed. The same damage area in a much larger plate would of course produce a smaller percentage decrease in overall strength. The residual strength factors quoted in these results should therefore not be interpreted as absolute values, but as relative values for comparing different composite lay-ups. The test procedure is described in (b).

Four series of tests were run; the results are reported in (c). Three of the series evaluated the residual strength of three different lay-up

configurations after impacts at various speeds. To minimize the effects of slight variations from plate-to-plate in the thickness of the fabricated plates, each one of these three series was run on a group of three 6 x 6 in. plates cut from the same 12 x 12 in. plate that had been fabricated from prepreg tapes and cured in an autoclave (Ref. 5). One of the three 6 x 6 in. plates was tested in cylindrical bending in the virgin undamaged condition as a control specimen. The other two were first impacted at different speeds and then tested in cylindrical bending. In these three test series the residual strength factors are ratios of the measured strength of the damaged plates to the measured strength of the undamaged plate of the same group.

The fourth series of tests was all for the glass/epoxy $[0°_5/90°_5/0°_5]$ system. A larger number of damaged plates was available in this system than any other, since this system had been used in an extensive investigation of delaminated area versus impactor kinetic energy. Since not all these plates were cut from a single fabricated plate the thickness variations had to be accounted for. This was done by calculating a fictitious apparent flexural modulus E_f and an apparent maximum flexural stress σ_{max} for each damaged plate, calculated by elementary elastic cylindrical bending formulas as though the plate had not previously been damaged. Stiffness was determined by measuring central deflection under the loading wedge with a dial gage, and determining the slope dP/dw of the linear part of the plot of load P versus dial-gage deflection w. In some tests deflection was measured at three points across the width of the plate underneath the loading wedge, but very little variation in w was observed across the width. The residual stiffness and strength factors are then quoted as ratios of the calculated values to similarly calculated values for undamaged plates. If all the plates were of exactly the same thickness the maximum stress ratios would be equal to the maximum load ratios. The resulting modulus ratios and maximum stress ratios were then plotted versus delamination area of the damaged plates of the glass/epoxy $[0°_5/90°_5/0°_5]$ system. Each ratio closely follows a straight line plot, but the stiffness decrease is much smaller than the strength decrease. All these results are reported in (c).

In addition some plates were fabricated with mylar inserts that prevented interlaminar bonding over certain areas and thus simulated impact-induced delaminations. Results from cylindrical bending tests on these are given in

(d) and compared with results from impact-damaged plates. A few exploratory tests on other composite materials (graphite/epoxy and Kevlar/epoxy) are reported in (e).

(b) Cylindrical Bend Test Procedures

In each test the two edges selected for support were chosen so that the plate was tested in the stronger orientation. That is, with 0° defined as the direction perpendicular to the supports and the upper loading wedge, the outer ply orientation θ always satisfied $0 \leq \theta \leq 45°$.

Figure 12 shows a series of photographs documenting the progressive failure of a $[30°_5/0°_5/30°_5]$ angle-ply plate. The photo on the upper left in Fig. 12 shows the back side of the plate after impact, before the cylindrical bend test. The photo on the upper right shows it after fracture in cylindrical bending. The vertical dark strip in this picture is the region of fiber fracture under the wedge. The photo on the lower left in Fig. 12 shows the broken plate, the supports and the loading wedge. Below the plate a mirror reflects the under side of the plate. The sequence 1 through 9 of pictures on the right were obtained by using the mirror. An edge delamination begins in Photo 2 and is clearly visible in Photo 3. Fiber fracture under the wedge is clearly apparent in Photo 7 but probably began a little earlier.

Figure 13 is a copy of the recorded load-deflection trace for the test shown in Figure 12. The trace is quite linear up to the point marked (2). The numbers on the trace correspond to the photo numbers in Figure 12. Thus Point 2 marks the initiation of edge delamination, and Point 7 corresponds to the first clearly visible fiber fracture under the wedge.

The "strength" of the plate was taken as the maximum load P_{max} (780 lb in Fig. 13), and the residual strength factor is reported as $P_{max}/P°_{max}$, where $P°_{max}$ is for the undamaged plate.

The two edge supports are each attached to the foundation by a single pin parallel to the 0° direction (perpendicular to the supports). The edge supports are free to rotate about this pin, so that no twisting moment is applied to the plates. The loading wedge is also free to rotate about its vertical axis, which it does to some extent with the angle-ply plates, as is evident from the fiber fracture direction in the photo on the upper right in Figure 12.

STATIC BEND TEST OF GLASS EPOXY PLATES

PLATE 19F (BACK SIDE) WITH PRIOR IMPACT DAMAGE

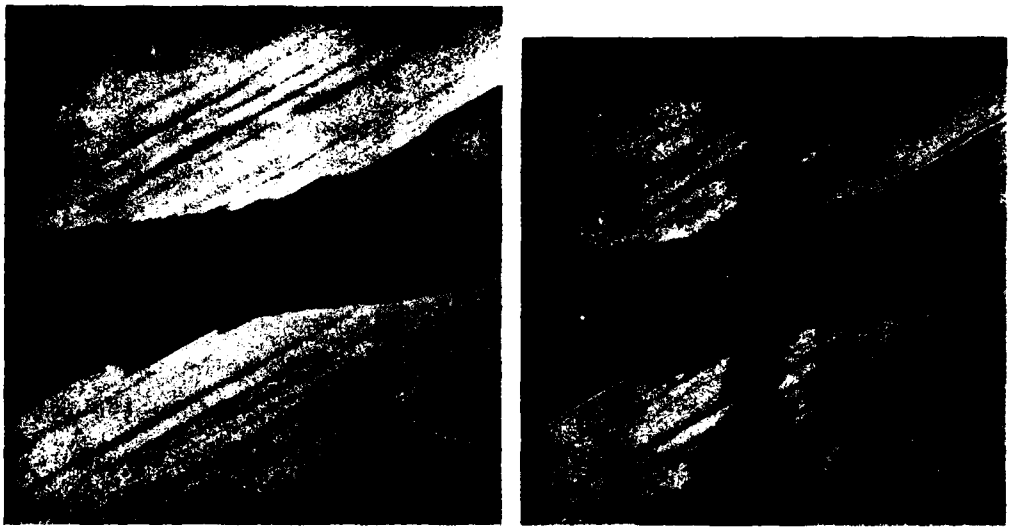

STATIC BEND TEST SEQUENCE [BACK SIDE OF PLATE SPECIMEN]

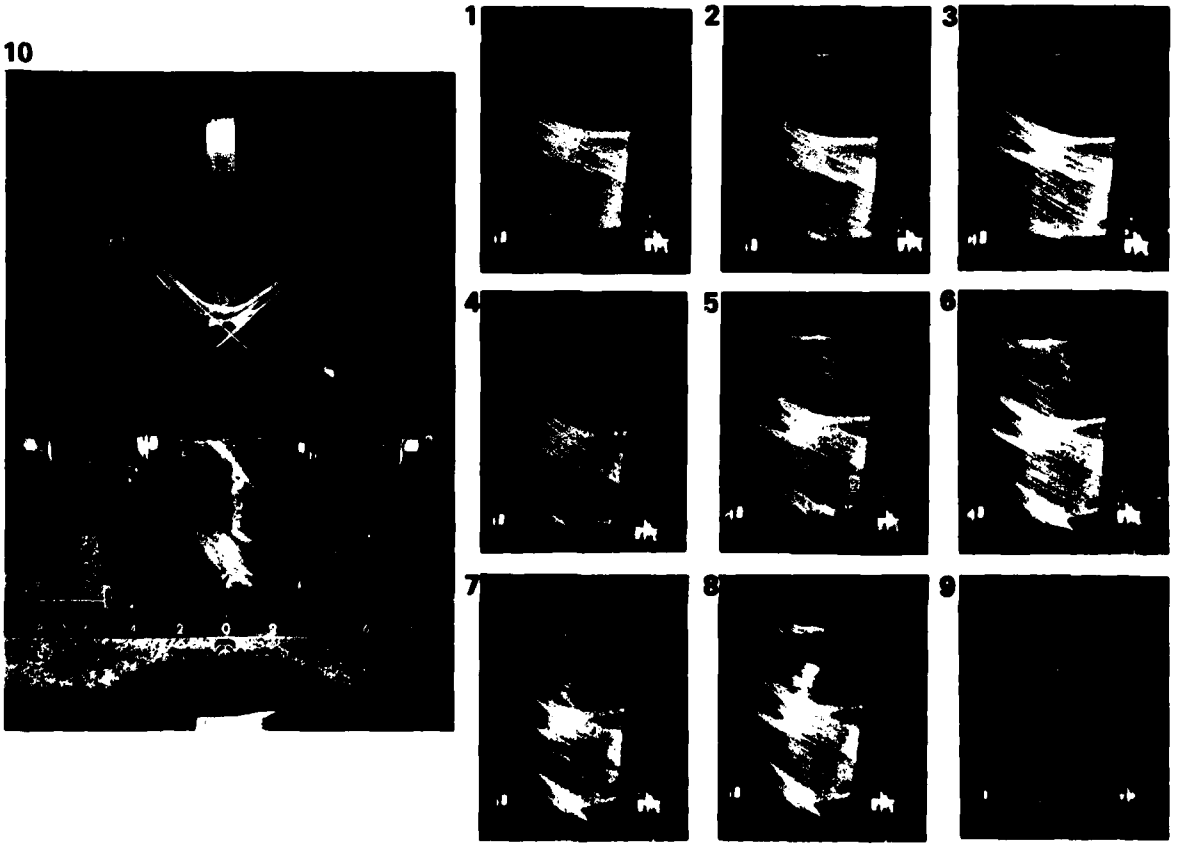

Figure 12.

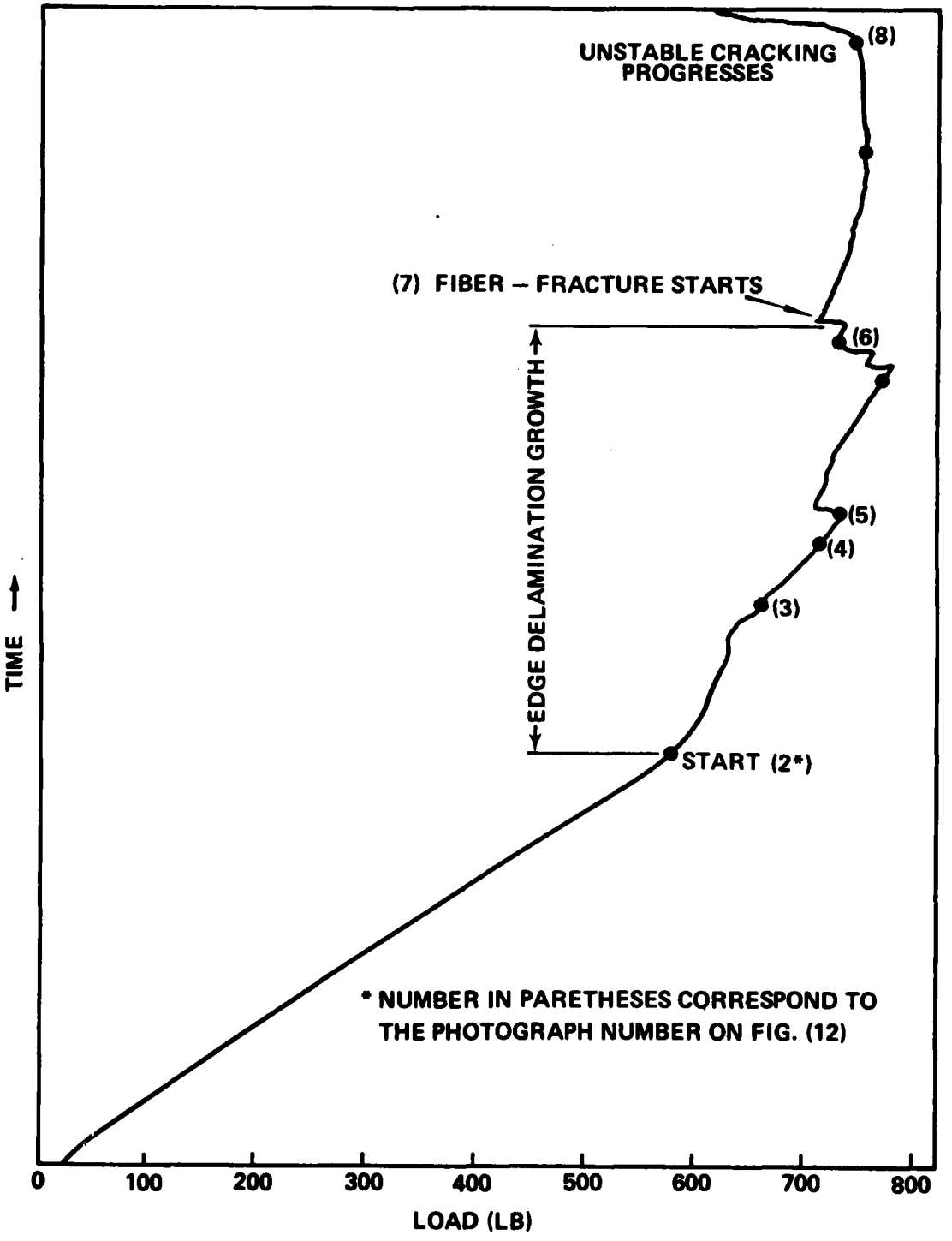

Figure 13. Load – Time Record For Plate No. 19F Tested at Constant Deflection Rate

The bending test fixture was mounted in the testing frame of a Tinius Olsen testing machine. Load was recorded from the load cell of the testing machine.

(c) Test Results

The four series of tests on glass/epoxy plates were as follows:

Series 1

Stacking sequence was $[30°_5/\phi°_5/30°_5]$ maintaining the outer fibers at ϕ = 30° relative to the axis perpendicular to the supports while the core fiber orientation was changed in 15° increments from ϕ = 0° to ϕ = -60°. For each orientation an undamaged plate and two plates that had been impacted at speeds of approximately 150 ft/sec and 300 ft/sec were tested in cylindrical bending. Results are shown in Table 2.

TABLE 2. SERIES 1, VARYING CORE ORIENTATION

Stacking Sequence	Plate number	Impact Velocity (ft/sec)	Failure Load (lb)	Residual Strength Factor $P_{max}/P°_{max}$
$[30°_5/0°_5/30°_5]$	D	0	1280	1.
	E	151	1050	0.82
	F	306	780	0.61
$[30°_5/-15°_5/30°_5]$	D	0	1340	1.
	E	145	1290	0.96
	F	312	1080	0.81
$[30°_5/-30°_5/30°_5]$	D	0	1300	1.
	E	143	1260	0.97
	F	307	765	0.59
$[30°_5/-45°_5/30°_5]$	D	0	1200	1.
	E	152	1140	0.96
	F	301	810	0.64
$[30°_5/-60°_5/30°_5]$	D	0	1300	1.
	E	146	1220	0.94
	F	309	420	0.32

Series 2

Stacking sequence was $[\theta°_5/(90°-\theta_5)/\theta°_5]$ keeping the core ply always at 90° to the outer ply and changing the outer ply orientation in 15° increments from θ = 0° to θ = 45°. For each orientation an undamaged plate and plates

previously impacted at about 150 ft/sec and 300 ft/sec were tested in cylindrical bending. Results are reported in Table 3.

TABLE 3. SERIES 2, VARYING OUTER PLY ORIENTATION

Stacking Sequence	Plate number	Impact Velocity (ft/sec)	Failure Load (lb)	Residual Strength Factor P_{max}/P°_{max}
$[0^{\circ}_5/90^{\circ}_5/0^{\circ}_5]$	D	0	2750	1.
	E	151	2400	0.87
	F	296	1150	0.42
$[15^{\circ}_5/-75^{\circ}_5/15^{\circ}_5]$	D	0	2130	1.
	E	146	1940	0.91
	F	305	1120	0.53
$[30^{\circ}_5/-60^{\circ}_5/30^{\circ}_5]$	D	0	1300	1.
	E	146	1220	0.94
	F	309	420	0.32
$[45^{\circ}_5/-45^{\circ}_5/45^{\circ}_5]$	D	0	750	1.
	E	149	670	0.89
	F	308	550	0.73

Table 2 shows only a weak dependence on core fiber orientation. The second series in Table 3 shows, as would be expected, a significant dependence of the undamaged plate strength on outer ply orientation, with the strongest plates having $\theta = 0^{\circ}$, but no conclusive dependence of the residual strength reducton factor on outer ply orientation.

Series 3

The third series studied the effect of changing the number of plies in each lamina of a crossply arrangement. Results are reported in Table 4.

TABLE 4. SERIES 3, VARYING STACKING SEQUENCE

Stacking Sequence	Plate number	Impact Velocity (ft/sec)	Failure Load (lb)	Residual Strength Factor P_{max}/P°_{max}
$(0°/90°/0°---)_{15}$	D	0	1420	1.
	E	148	1180	0.83
	F	298	820	0.58
$(0°_3/90°_3/---)_{15}$	D	0	2280	1.
	E	148	2200	0.97
	F	299	1320	0.58
$[0°_5/90°_5/0°_5]$	D	0	2750	1.
	E	151	2400	0.87
	F	296	1150	0.42

Table 4 shows that increasing the number of plies in the outermost lamina ($\theta = 0°$) of the 0°/90° plates significantly enhances the undamaged plate strength, but again has no conclusive effect on the strength-reduction factor. The small value of 0.42 for the residual strength factor of the $[0°_5/90°_5/0°_5]$ plate No. F impacted at the higher velocity may have been caused by the fact that the impact-induced delamination had extended almost to the boundary in this case.

Series 4

Residual apparent strength and stiffness for several $[0°_5/90°_5/0°_5]$ plates were calculated. Results are tabulated in Table 5 and plotted in Figure 14. Formulas for the apparent flexural modulus E_f, and maximum bending stress are shown below, based on elementary beam bending formulas and calculated as though the plate had not been damaged.

$$\text{Apparent } E_f = \frac{(dP/dw)L^3}{4bh^3} \tag{1}$$

$$\text{Apparent } \sigma_{max} = \frac{3P_{max}L}{2bh^2} \tag{2}$$

where dP/dw is the slope of the linear part of the plot of load P versus central dial-gage-measured deflection, L is the length between supports, b is the width and h is the thickness of the plate.

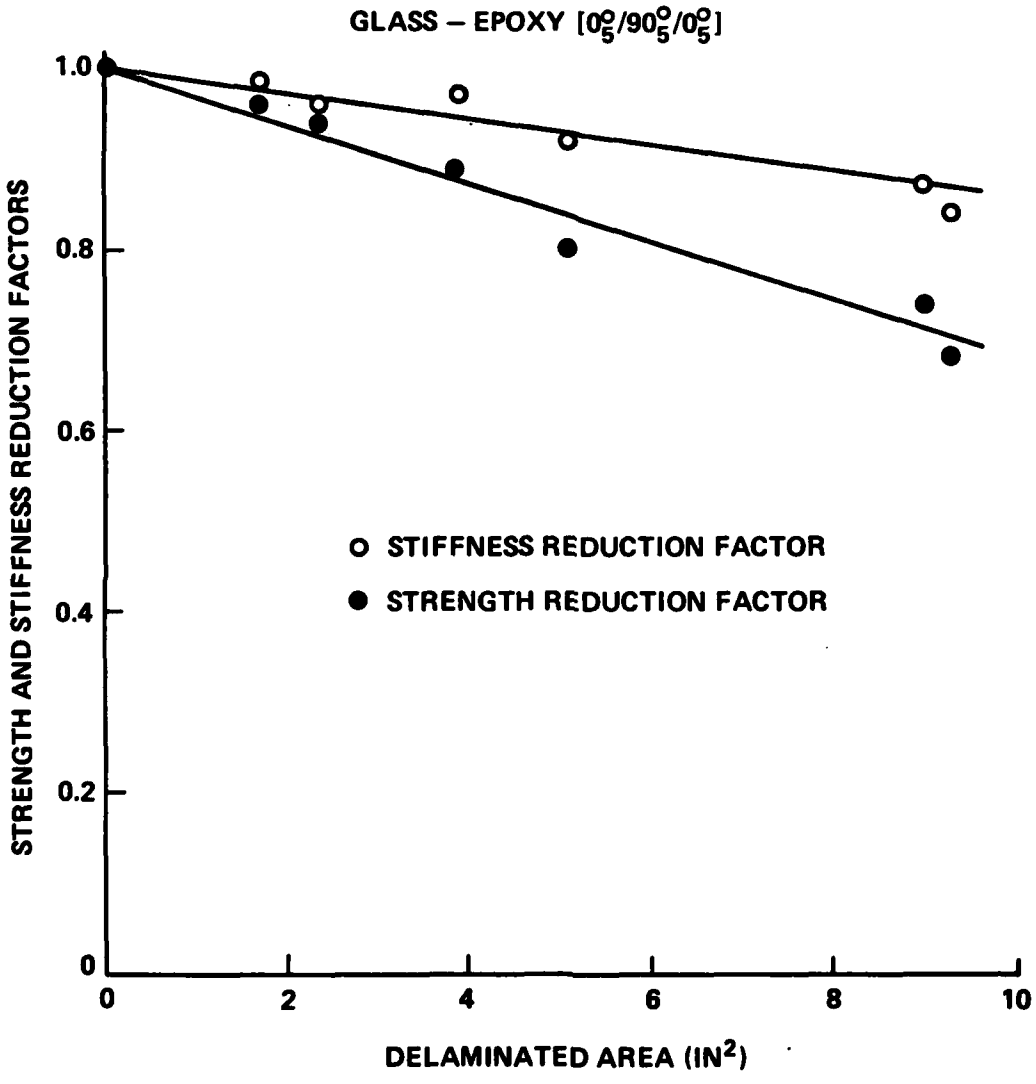

Figure 14. Stiffness And Strength Reduction Factors in [$0_5^\circ/90_5^\circ/0_5^\circ$] Glass – Epoxy Plates Versus Delaminated Area.

TABLE 5. SERIES 4, STACKING SEQUENCE $[0°_5/90°_5/0°_5]$

Plate number	Impact Velocity (ft/sec)	Apparent Flexural Stiffness $E_f x10^{-6}$ psi	Apparent Flexural Strength $\sigma_{max} x10^{-4}$ psi	Stiffness Reduction Factor $E_f/E°_f$	Strength Reduction Factor $\sigma_{max}/\sigma°_{max}$	Total Delam. Area (in^2)
1-C	0	6.1	16.64	1.0	1.0	0
1-A	100	6.03	16.0	0.99	0.96	1.66
1-B	180	5.94	14.87	0.97	0.89	3.89
4-A	156	5.86	15.58	0.96	0.94	2.32
4-B	198	5.61	13.17	0.92	0.79	5.10
4-C	247	5.11	11.24	0.84	0.68	9.30
4-D	247	5.30	12.34	0.87	0.74	9.03

As is shown in Table 5 and Figure 14, in the glass/epoxy $[0°_5/90°_5/0°_5]$ system both the stiffness reduction factor $E_f/E_f°$ and the strength reduction factor $\sigma_{max}/\sigma°_{max}$ plot as linear functions of the delaminated area, but the stiffness reduction is much less than the strength reduction.

(d) Simulated Plate Damage Studies

A number of glass/epoxy $[0°_5/90°_5/0°_5]$ plates were fabricated with 0.005-inch-thick mylar inserts that prevented interlaminar bonding over certain areas to simulate impact-induced delaminations over those areas. Table 6 summarizes the cases tested in this preliminary investigation for residual strength and stiffness in cylindrical bend tests by the procedure of (b). For each plate, one 6 x 6 in. quadrant of the 12 x 12 in. plate was fabricated without an insert as a control specimen, while the other three quadrants had inserts with the same total area. For example, after the 12 x 12 in. Plate No. 2 was cut into four plates, 2A had no insert while each of the other three had two inserts of area 4 $in.^2$, one in each interface, for a total simulated delaminated area of 8 $in.^2$. In Plate 2-B each insert was a 2 x 2 in. square, while in 2-C and 2-D each insert was a 1 x 4 in. rectangle. In 2-C the long edge of the rectangle was parallel to the outer-layer fiber direction while in Plate 2-D the long edge was perpendicular to the outer-layer fiber direction. Plate 3 was fabricated similarly but with each insert area of 8 $in.^2$ (2.83 x 2.83, 2 x 4 and 4 x 2).

TABLE 6. STRENGTH AND STIFFNESS REDUCTION FACTORS FOR $[0°_5/90°_5/0°_5]$ GLASS/EPOXY WITH SIMULATED DELAMINATION OVER EQUAL RECTANGULAR AREAS IN TWO INTERFACES

Plate number	Artificial Delamination Area ($in.^2$)	Apparent Flexural Modulus $E_f x10^{-6}$ psi	Apparent Flexural Strength $\sigma_{max} x10^{-4}$ psi	Stiffness Reduction Factor $E_f/E_f°$	Strength Reduction Factor $\sigma_{max}/\sigma°_{max}$
2-A	0	5.74	17.16	1.0	1.0
2-B*	4+4=8	5.40	10.15	0.94	0.59
2-C*	4+4=8	5.60	12.98	0.98	0.77
2-D*	4+4=8	5.68	12.60	0.99	0.73
3-A	0	5.66	16.81	1.0	1.0
3-B*	8+8=16	4.81	7.52	0.85	0.45
3-C*	8+8=16	5.00	12.10	0.88	0.72
3-D*	8+8=16	4.76	6.24	0.84	0.37

* Plates 2-B and 3-B have square inserts. Plates 2-C and 3-C have long edge parallel to outer-layer fiber direction, while 2-D and 3-D have long edge perpendicular to outer-layer fibers.

These plates were tested in cylindrical bending in the same way as described in (b). Figure 15 compares a plot of the strength reduction factor versus total delaminated area for these simulated delaminations with the similar plot for the damaged plates (replotted from Figure 14). It was observed that in the simulated-damage plate the failure process began on the compression side of the plate with additional delamination extending in the direction parallel to the outer fibers as shown in the sketches for Plates 2-C and 2-D in Figure 15. This delamination extended to the edge of the plate almost immediately, and the load at the initiation of this additional delamination was the maximum load attained.

This observation, that the failure always began on the compression side, when the two interface delaminations were of equal area indicated that different results might have been obtained with the impact-damaged plates (which had unequal areas at the two interfaces) depending on which of the two delaminated areas was on the compression side. This should be controlled in any further tests of impact damaged plates. Another series of plates were fabricated with unequal areas at the two interfaces to more nearly simulate the previously-tested impact-damaged plates. These plates had inserts of the

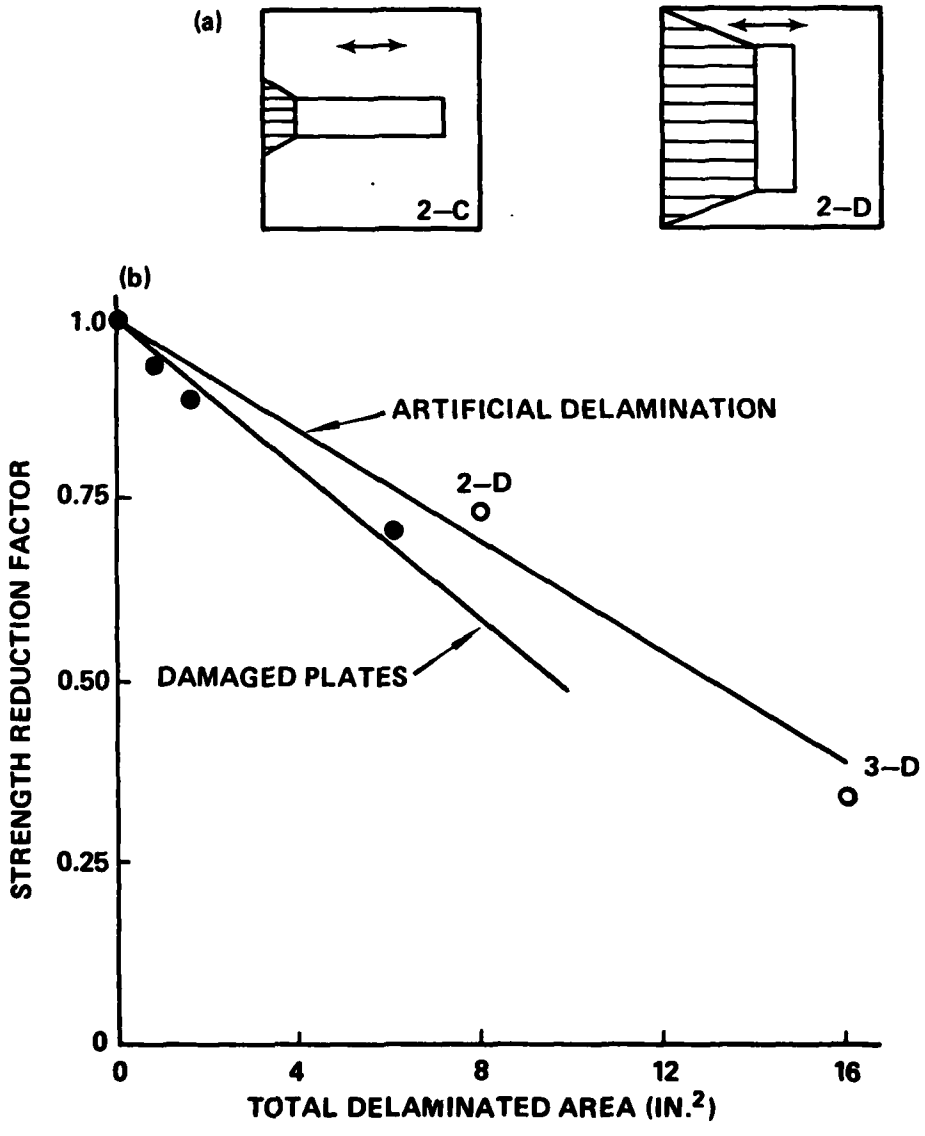

Figure 15. Artificial Delaminations (Rectangular)
(a) Additional Delamination on Compression Side.
(b) Strength Reduction Factors Versus Delaminated Area For Equal Artificial Delaminations in Front and Back Interfaces Compared to Impact–Damaged Plates.

same shape and area as the impact-induced delaminations in Plates 4A, 4B, and 4C.

Table 7 compares the stiffness reduction factors and strength reduction factors for these three plates with the impact damaged plates tested in the same configuration (with the larger delamination in the bottom interface). The agreement is quite good for the stiffness reduction factors and almost exact for the strength reduction factors. Evidently the reduction in stiffness and strength is directly related to the delamination, and not to other possible impact damage mechanisms.

TABLE 7
STIFFNESS AND STRENGTH REDUCTION FACTORS FOR IMPACT-DAMAGED PLATES COMPARED TO PLATES WITH ARTIFICIAL DELAMINATIONS OF THE SAME SIZE AND SHAPE. ALL PLATES ARE $[0°_5/90°_5/0°_5]$ GLASS/EPOXY. (plate numbers in parentheses)

Stiffness Reduction Factors		Strength Reduction Factors	
Impact Damaged	Artificial Delamination	Impact Damaged	Artificial Delamination
0.96 (4-A)	0.94 (AD-3-A)	0.94 (4-A)	0.95 (AD-3-A)
0.92 (4-B)	0.94 (AD-3-B)	0.79 (4-B)	0.78 (AD-3-B)
0.84 (4-C)	0.94 (AD-3-C)	0.68 (4-C)	0.65 (AD-3-C)

(e) Other Composite Systems Studied

In addition to the glass/epoxy system studies reported above, exploratory studies were made on graphite/epoxy and Kevlar/epoxy plates. Fiber and matrix materials for the system studied are listed in Table 8.

TABLE 8. FIBER AND MATRIX MATERIALS

Material	Fiber	Matrix	Supplier
Graphite/Epoxy	THORNEL 300	PR-322 Epoxy	3M Co.
Kevlar/Epoxy	KEVLAR 49	PR-328 Epoxy	3M Co.

Plate specimens were fabricated from prepreg tapes following procedures similar to those for glass/epoxy specimens and recommendations supplied by the tape manufacturers. In order to test plates of comparable thickness it was necessary to use more layers of graphite and Kevlar (15 for glass, 27 for graphite, and 17 or 18 for Kevlar). Fiber volume fractions in the final composites were approximately 0.55 for graphite and 0.5 for Kevlar. Only 0°/90° specimens were fabricated in this exploratory series in order to compare with the most extensive glass/epoxy data base available. Two configurations were fabricated: (1) alternating crossply, and (2) one with only two interfaces, $[0°_5/90°_5/0°_5]$ for glass, $[0°_6/90°_6/0°_6]$ for Kevlar and $[0°_9/90°_9/0°_9]$ for graphite as summarized in Table 9.

The threshold velocity for perforation by a blunt-ended cylindrical steel projectile 25 mm long by 10 mm in diameter was substantially lower for both the graphite/epoxy and Kevlar/epoxy plates tested than it was for the glass/epoxy plates. To compare residual strengths after impact at subperforation speeds it was necessary to use a lower range of speeds than in the glass/epoxy plates reported in (c). Maximum loads P_{max} and residual load factors $P_{max}/P°_{max}$ are reported in Table 9, for cylindrical bending tests as described in (b).

Quite different results were obtained from the different systems for the strength of the undamaged control plates. The glass/epoxy system with 2 interfaces, Plate No. 3-D reached a maximum load of 2750 lb, 1.94 times the maximum load of the alternating crossply Plate No. 1-D. In the graphite/epoxy system the situation was just the reverse with the maximum load of 3200 lb for the alternating crossply being 2.18 times that for the plate with only two interfaces. No control specimen was tested for the Kevlar/epoxy plate with two interfaces, but a comparison of the damaged plates impacted at about 150 ft/sec. indicates that the two-interface plate is only slightly stronger than the alternating ply plate. Since it had 18 layers of fibers, as compared with 17 for the alternating-ply plate, there is not a significant difference in strength for the two configurations in Kevlar/epoxy.

Figure 16 compares curves of load versus central deflection in cylindrical bending tests on three impact damaged plates, one from each system with two interfaces, all impacted at about the same speed of 150 ft./sec. The glass/epoxy curve is approximately linear up to the maximum load of 2400 lb.

at a deflection of 0.61 in. while the Kevlar is markedly nonlinear above a deflection of about 0.1 in. The graphite/epoxy shows a load drop at about 0.08 in. deflection, but then continues along another approximately linear curve almost to its maximum load. The maximum load attained is significantly higher for the glass/epoxy plate than for either the graphite/epoxy or Kevlar/epoxy plate in this configuration.

TABLE 9 MAXIMUM LOADS AND RESIDUAL STRENGTH FACTORS COMPARED FOR PLATES OF THREE MATERIALS

Material	Stacking Sequence	Specimen No.	Impact velocity (ft/sec)	Maximum Load P_{max} lb.	Residual Strength Factor P_{max}/P°_{max}
		Alternating Ply			
Glass-Epoxy	$[0°/90°/0°---]_{15}$	1-D	0	1420	1.0
		1-E	148	1180	0.83
		1-F	298	820	0.58
Kevlar-Epoxy	$[0°/90°/0°---]_{17}$	Kev-2-a	0	1000	1.0
		Kev-2-d	152	910	0.91
		Kev-2-b	252	780	0.78
Graphite-Epoxy	$[0°/90°/0°---]_{27}$	Gr-2-c	0	3200	1.0
		Gr-2-a	152.	2120	0.66
		Gr-2-b	178	1900	0.59
		Two Interface			
Glass-Epoxy	$[0°_5/90°_5/0°_5]$	3-D	0	2750	1.0
		3-E	151.	2400	0.87
		3-F	296.	1150	0.42
Kevlar-Epoxy	$[0°_6/90°_6/0°_6]$	----	0	----	----
		Kev-1-a	112.	1190	----
		Kev-1-d	150.	1020	----
Graphite-Epoxy	$[0_9/90°_9/0_9]$	Gr-1-c	0	1470	1.0
		Gr-1-a	150.	925	0.63
		Gr-1-b	178.	920	0.63

With the alternating crossply plates, however, the situation is again reversed, just as it was for the undamaged plates, Figure 17 shows that the

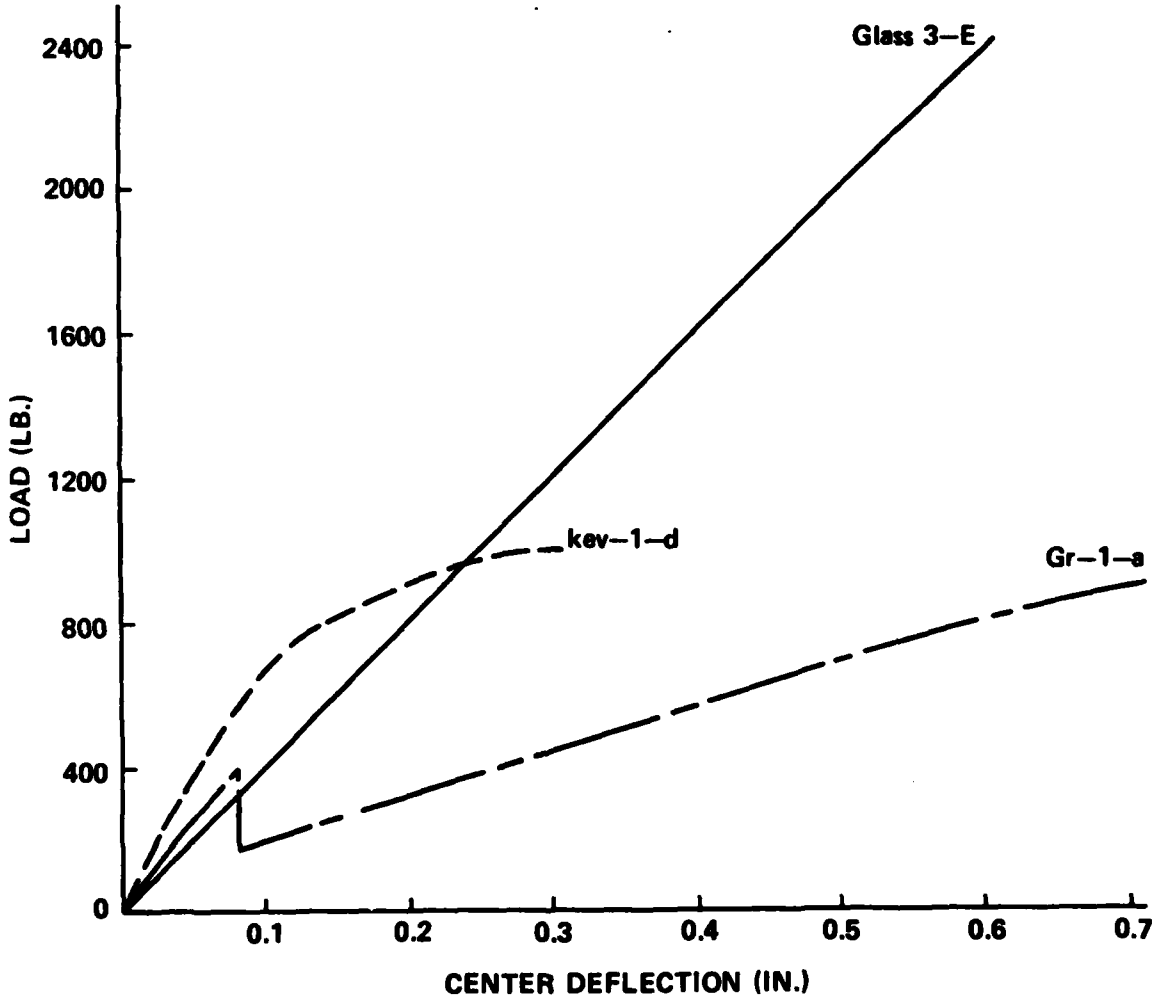

Figure 16. Load – Deflection Curves For Two Interface Plates of Three Materials After Impact at About 150 ft/sec.

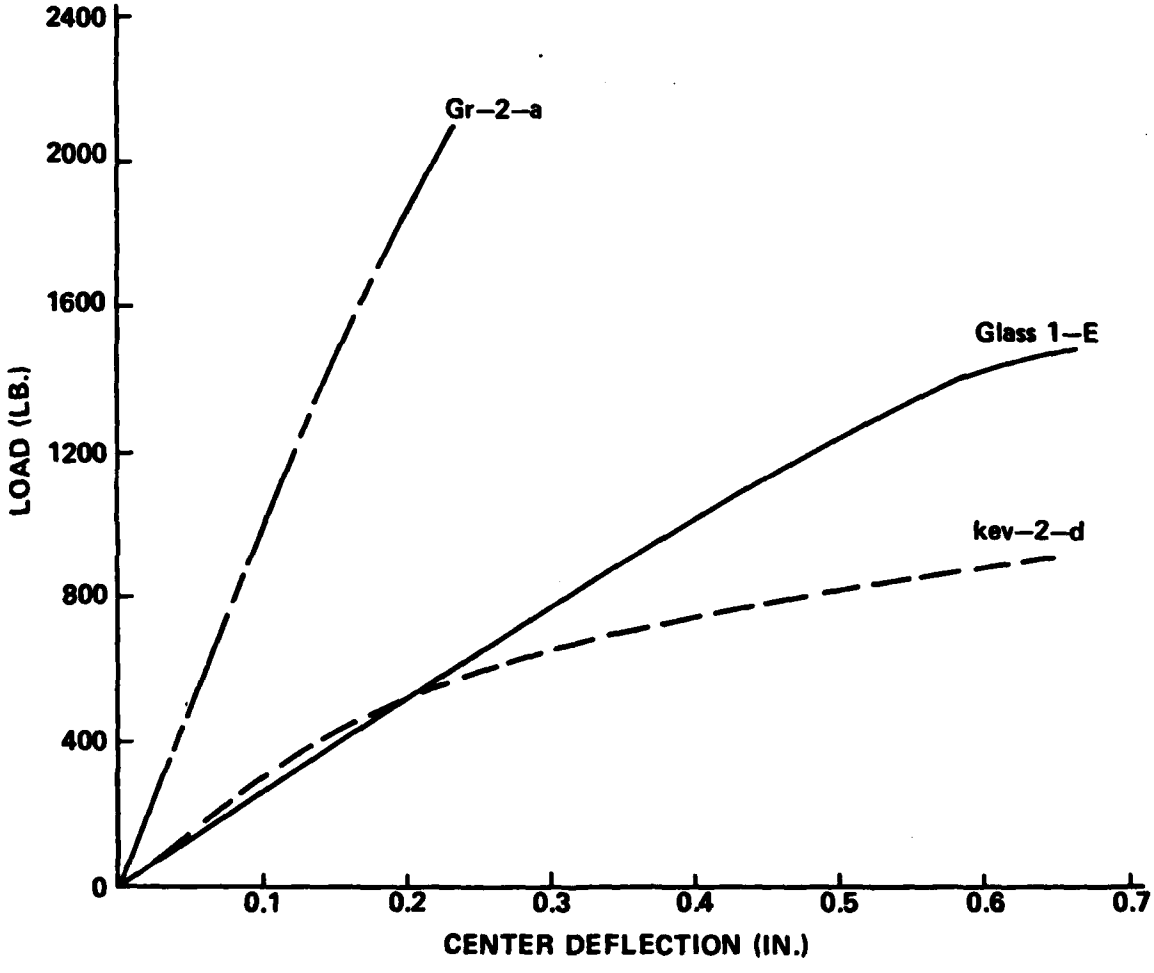

Figure 17. Load Deflection Curves For Alternating Ply Plates of Three Materials After Impacts at About 150 ft/sec.

graphite/epoxy alternating crossply plate showed significantly higher residual strength and stiffness than either of the other two alternating crossply systems.

(f) Summary and Conclusions from Residual Strength Tests

The static three-point cylindrical bending tests on damaged glass/epoxy laminates with two interfaces showed little dependence of strength on the core ply orientation. While the strength of undamaged plates showed a significant dependence both on the outer ply orientation and on the number of fiber layers in the outer plies, neither of these factors had a conclusive effect on the fraction of the initial strength retained after impact.

A series of tests on $[0°_5/90°_5/0°_5]$ glass/epoxy plates showed that both the strength reduction factor and the stiffness reduction factor plot as linear functions of the delaminated area, but the stiffness reduction is much less than the strength reduction. Therefore evaluation procedures based on stiffness measurements will give an underestimate of the damage.

Some tests with impact-induced delamination simulated by mylar inserts of the same shape, position and area as actual impact-induced delaminations produced strength reductions and stiffness reductions correlating closely with the reduction factors in actual damaged plates. This is evidence that the important damage mechanism in these subperforation velocity impacts is the delamination and not some other possible damage mechanisms.

Exploratory tests were made with two other material systems (graphite/epoxy and Kevlar/epoxy). The threshold perforation velocity was substantially lower in both these system than in glass/epoxy for the 0°/90° plates tested of comparable thickness. Stacking sequence effects on both undamaged plate strength and residual strength after impact were strikingly different in the graphite/epoxy plates from the effects in glass/epoxy. For glass/epoxy the undamaged $[0°_5/90°_5/0°_5]$ plates with two interfaces reached a maximum load in cylindrical bending 1.94 times the load attained with 0°/90° alternating ply plates having the same total number of plies. With graphite/epoxy the situation was just the reverse. The maximum load in alternating ply plates was 2.18 times the load attained with two interfaces having the same total number of plies. This investigation of other materials was too limited to warrant attaching importance to the specific numerical values cited, but the striking qualitative differences indicate that

additional studies should be made in the other systems, and that it is hazardous to try to infer the behavior of the other systems from observations of the glass/epoxy system.

LITERATURE CITED

1. Mente, L. J., and Lee, W. N., "DEPROP - A Digital Computer Program for Predicting Dynamic Elastic-Plastic Response of Panels to Blast Loading," AFATL-TR-76-71, USAF Armament Laboratory, Eglin AFB, Florida, June 1976.
2. Sierakowski, R. L., Ross, C. A., Malvern, L. E., and Cristescu, N., "Studies on the Penetration Mechanics of Composite Plates," Final Rept., Grant No. DAAG29-76-G-0085, US Army Res. Off., N.C., December 1976.
3. Bathe, K. J., Wilson, E. L., and Peterson, F. E., "SAPIV, A Structural Analysis Program of Static and Dynamic Response of Linear Systems," EERC 73-11 Earthquake Engineering Res. Cent., University of California, Berkeley, California, April 1974.
4. Malvern, L. E., Sierakowski, R. L., Ross, C. A. and Cristescu, N., "Impact Failure Mechanisms in Fiber-Reinforced Composite Plates, in High Velocity Deformation of Solids, eds Kawata, K. and Shiori, J., Springer-Verlag, Berlin 1978, pp 120-130 (Proceedings of IUTAM Symposium, Tokyo 1977).
5. Takeda, N., "Experimental Studies of the Delamination Mechanisms in Impacted Fiber-Reinforced Composite Plates," Ph.D. Dissertation, University of Florida, 1980.
6. Takeda, N., Sierakowski, R. L. and Malvern, L. E., "Studies of Impacted Glass Fiber Reinforced Composite Laminates," SAMPE Quarterly, Vol. 12, No.2, January 1981, pp 9-17.
7. Sierakowski, R. L., Ross, C. A. and Malvern, L. E., "Studies on the Fracture Mechanisms in Partially Penetrated Filament Reinforced Laminated Plates," Final Report on U.S. Army Research Office Grant DAAG 29-79-G-0007, University of Florida, Gainesville, FL December 31, 1981.

(The reverse side of this page is blank.)

UNCLASSIFIED

SECURITY CLASSIFICATION OF THIS PAGE (When Data Entered)

REPORT DOCUMENTATION PAGE		READ INSTRUCTIONS BEFORE COMPLETING FORM
1. REPORT NUMBER	2. GOVT ACCESSION NO. AD-A113 249	3. RECIPIENT'S CATALOG NUMBER
4. TITLE (and Subtitle) STUDIES ON THE FRACTURE MECHANISMS IN PARTIALLY PENTRATED FILAMENT REINFORCED LAMINATED PLATES		5. TYPE OF REPORT & PERIOD COVERED Interim Technical Report No. 1
		6. PERFORMING ORG. REPORT NUMBER
7. AUTHOR(s) R. L. Sierakowski, C. A. Ross, L. E. Malvern, H. W. Doddington		8. CONTRACT OR GRANT NUMBER(s) DAAG29-79-G0007
9. PERFORMING ORGANIZATION NAME AND ADDRESS Department of Engineering Sciences, University of Florida, Gainesville, Florida 32611		10. PROGRAM ELEMENT, PROJECT, TASK AREA & WORK UNIT NUMBERS
11. CONTROLLING OFFICE NAME AND ADDRESS U. S. Army Research Office, Post Office Box 12211, Research Triangle Park, North Carolina 27709		12. REPORT DATE 30 January 1982
		13. NUMBER OF PAGES 43
14. MONITORING AGENCY NAME & ADDRESS(if different from Controlling Office)		15. SECURITY CLASS. (of this report) UNCLASSIFIED
		15a. DECLASSIFICATION/DOWNGRADING SCHEDULE

16. DISTRIBUTION STATEMENT (of this Report)

APPROVED FOR PUBLIC RELEASE: DISTRIBUTION UNLIMITED

17. DISTRIBUTION STATEMENT (of the abstract entered in Block 20, if different from Report)

18. SUPPLEMENTARY NOTES

The views, opinions, and/or findings contained in this repor are those of the authors and should not be construed as an official department of the army position, policy, or decision, unless so designated by other documentation.

19. KEY WORDS (Continue on reverse side if necessary and identify by block number)

Solid Mechanics	Energy Absorption	Residual Strength
Ballistic Impact	Dynamic Fracture	Beams
Composites	Interlaminar Shear	Plates

20. ABSTRACT (Continue on reverse side if necessary and identify by block number)

This research program has investigated fracture mechanisms in centrally impacted glass/epoxy composite plates to establish design guidelines for plates to resist such impacts. Three topics investigated but not previously reported in journal articles are included in this report: (]) the development of a multi-channel transient recording system, (2) analysis of interlaminar shear stresses in the elastic flexural wave, and (3) residual strength and stiffness studies of damaged plates. The last topic included exploratory measurements on graphite/epoxy and Kevlar/epoxy plates.

DD FORM 1 JAN 73 1473 EDITION OF 1 NOV 65 IS OBSOLETE S/N 0102-014-6601

UNCLASSIFIED


DAT
ILM